

RESEARCH

Open Access



Genetic implications of Th/U, Th/K, and U/K ratios for U mineralizations: A case study from El-Missikat and El-Erediya shear zones, Eastern Desert, Egypt

Mahmoud Abdel-Hakeem^{1*}, Mohamed El-Tahir¹, Ehab Abu Zeid² and Hassan Rageh¹

Abstract

The current work is an attempt to reveal the possible utilization of the radiometric measurements to build-up a complete genetic scenario for magmatic, hydrothermal, and supergene uranium mineralization. For this purpose, ground gamma-ray survey was performed through the exploratory tunnels dug perpendicular to El-Missikat and El-Erediya shear zones, the Central Eastern Desert of Egypt. Contents of U, Th, and K were measured for the host pink granite (e.g., avg. 15.94 U ppm, 35.62 Th ppm, and 6.63% K), alteration zones (brecciation, silicification, greisenization, kaolinization and hematitization) (e.g., avg. 124.01 U ppm, 63.67 Th ppm, and 3.13% K), and mineralized silica veins (e.g., avg. 312.65 U ppm, 92.22 Th ppm, and 2.62% K). All of these data were graphically represented as correlation plots of Th vs. U, Th/U vs. U, Th vs. K, and U/K vs. Th/K. The overall results indicate magmatic, hydrothermal, and supergene sources of El-Missikat and El-Erediya U mineralization. The magma-derived U contents are enclosed mainly in the pink granite that is mostly characterized by normal Th/U (2.5–5) and Th/K ratios ($3-5 \times 10^{-4}$). The hydrothermal processes through the alteration zones and mineralized silica veins are reflected by the weak correlation of Th with U (e.g. $r = 0.13$ and -0.39), the strong negative correlation of Th/U ratio with U (e.g. $r = -0.82$), $2.5^2 \text{Th}/\text{U} > 0.1$, $\text{Th}/\text{K} > 5 \times 10^{-4}$, $\text{Th}/\text{K} < 3 \times 10^{-4}$, and the strong positive correlation of U/K with Th/K (e.g. $r = 0.91$) as well as the occurrence of thorite, columbite, xenotime and hydrothermal zircon ($0.5 > \text{Th}/\text{U} \leq 0.1$). Afterwards, the hydrothermal mineralization underwent some degrees of chemical weathering that resulted in supergene U mineralization whose fingerprints can be traced by the occurrence of secondary U minerals (e.g. kasolite and uranophane), Th/U ratios ≤ 0.1 , and the weak correlation between Th/K and U/K (e.g. $r = 0.39$ and -0.11).

Keywords El-Missikat mine, El-Erediya mine, U mineralization, Th/U ratio, Th/K ratio, U/K ratio

Introduction

U, Th, and K are considered to be large ion lithophile elements well-known for their radioactivity and heat production as well as the common occurrence, at relative abundances, in granites compared to the other rock types [8, 62]. They have a characteristic geochemical behavior (e.g. the incompatible magmatic fractionation of U and Th in relative to K and the post-magmatic mobilization of U and K compared to Th) under magmatic, hydrothermal, and supergene conditions (e.g [16, 18, 23, 24, 37, 47,

*Correspondence:

Mahmoud Abdel-Hakeem
mahmoud.sabry@sci.svu.edu.eg

¹ Department of Geology, Faculty of Science, South Valley University, Qena, Egypt

² Nuclear Materials Authority, Maadi, Cairo, Egypt



© The Author(s) 2023. **Open Access** This article is licensed under a Creative Commons Attribution 4.0 International License, which permits use, sharing, adaptation, distribution and reproduction in any medium or format, as long as you give appropriate credit to the original author(s) and the source, provide a link to the Creative Commons licence, and indicate if changes were made. The images or other third party material in this article are included in the article's Creative Commons licence, unless indicated otherwise in a credit line to the material. If material is not included in the article's Creative Commons licence and your intended use is not permitted by statutory regulation or exceeds the permitted use, you will need to obtain permission directly from the copyright holder. To view a copy of this licence, visit <http://creativecommons.org/licenses/by/4.0/>. The Creative Commons Public Domain Dedication waiver (<http://creativecommons.org/publicdomain/zero/1.0/>) applies to the data made available in this article, unless otherwise stated in a credit line to the data.

55, 59, 60], making them significant tracers in the geochemical exploration and mapping the hydrothermal and supergene alteration zones (e.g; [1, 13, 20, 26, 27, 36, 46, 48, 49, 51, 58, 64, 66, 67]). Apart from the other geochemical approaches such as fluid inclusions and whole rock geochemistry, the current work tries to build-up a radioelement ratio-based genetic scenario for vein-type uranium mineralizations by measuring Th/U, Th/K, and U/K ratios through host rocks, alteration zones, and U mineralized-veins. For this purpose, polymetallic, vein-type U mineralizations hosted by El-Missikat and El-Erediya pink granites, Eastern Desert of Egypt, were undertaken as a case study. The radioactivity of such localities was first discovered, under supervision of the Egyptian Authority of Nuclear Materials, using airborne gamma-ray survey during a project of uranium exploration between latitudes 25–27°N, through the Central Eastern Desert of Egypt [7]. This was followed by ground inspection of these anomalous sites, leading to dig a number of exploratory mining tunnels through the northwestern part of El-Missikat pluton and the southern part of El-Erediya pluton [3, 4, 10, 31, 35]).

Geological setting

El-Missikat (26° 28' 33" and 26° 29' 50" N and 33° 22' 6" and 33° 23' 6" E) and El-Erediya pink granites (26° 18' 35" and 26° 20' 2" N & longitudes 33° 28' 10" and 33° 29' 43" E) are exposed as oval-shaped plutons elongated in NNW and NW directions, respectively, through the Central Eastern Desert of Egypt (Fig. 1). These plutons along with the hosted U mineralizations attracted several discussions [3, 4, 4, 5, 9–12, 30–35, 39, 41–43, 53, 56, 57, 63]. Accordingly, both El-Missikat and El-Erediya plutons are post-orogenic, peraluminous, medium-to-coarse-grained, younger granitic intrusions composed mainly of perthite (31–50%), plagioclase feldspars (15–20%), and smoky quartz (20–35%), with small amounts of biotite and hornblende (1–3%). Structurally, ENE-WSW and NE-SW trending shear zones cross cut El-Missikat and El-Erediya pink granites, respectively. Moreover, the exploratory mining tunnels through the northwestern part of El-Missikat (Fig. 2) and the southern part of El-Erediya plutons (Fig. 3) revealed that the pink granite is intruded by 1.5 m thick aplite dike at the main adit and suffers brecciation, silicification, greisenization, hematitization, and kaolinization (Figs. 4, 5). Toward the center of shear zone, parallel sets of red to black, lenticular-shaped, siliceous veins invading the pink granite of El-Missikat and El-Erediya areas, were also exposed. They host well-developed fluorite along with U mineralizations, represented mainly by pitchblende, uranophane, autunite, and soddyite, with varied thickness from few centimeters up to 10 m. It is worth to mention that the

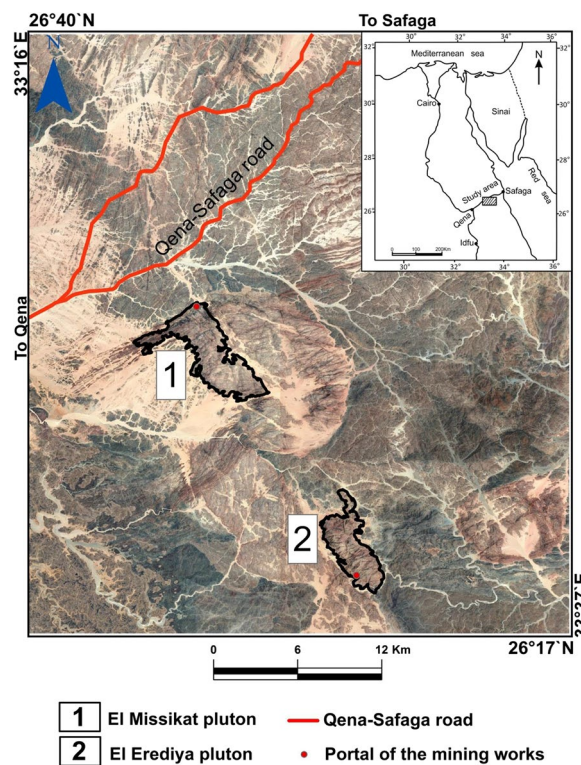


Fig. 1 Location map of El-Missikat and El-Erediya plutons showing the portal of the mining works

occurrence of pitchblende is less abundant due to its highly labile behavior under chemical weathering. So, the secondary U minerals, mostly yellowish to greenish in color, are commonly perceived during the field observations (Figs. 6, 7).

Methodology

The distribution of U (ppm), Th (ppm), and ^{40}K (%) was determined for fresh granite, alteration zones, and radioactive siliceous veins within the exploratory tunnels by handheld gamma-ray spectrometer (RS-230). This device is characterized by BGO “bismuth germanate oxide” detector by which the radioelement concentrations are directly measured without the need for calibration resources. The background was measured on the surface for the surrounding fresh granite, out of the exploratory tunnels, at 7.4 ppm U, 26.1 ppm Th, and 6% K. The radioactive measurements were systematically taken through successive profiles, 50 cm/read along each profile, that are perpendicular to shear zone and arranged at 1 m long distance, starting from the main adit until reaching the subsequent drifts (D_I and D_{II} at El-Missikat and D_{II} and D_{III} at El-Erediya). The total count of these measurements for fresh granite, brecciation, greisenization, silicification, kaolinization, hematitization, brecciated and massive

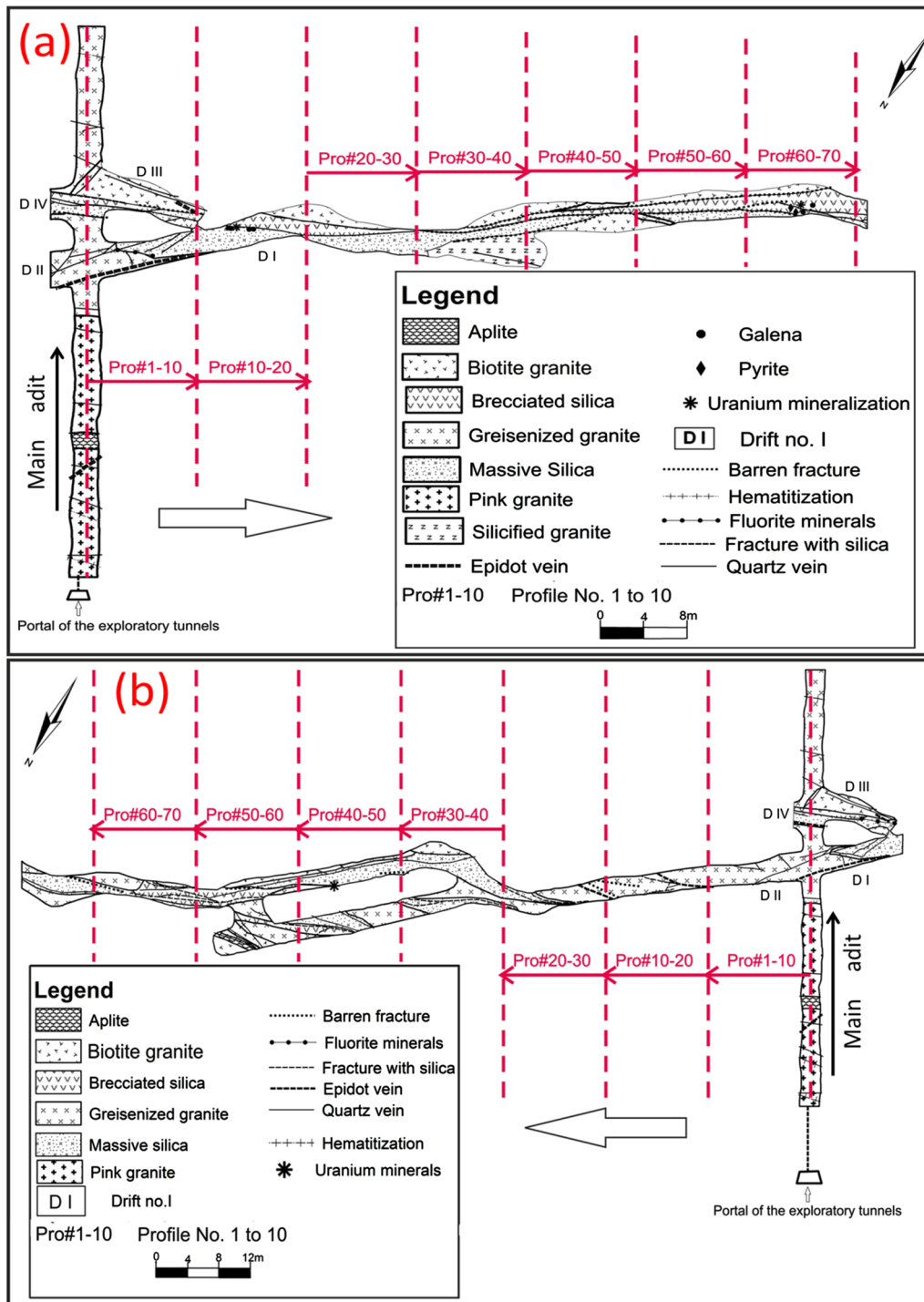


Fig. 2 Geological maps of drifts# D I&D III **a** and D II **b** through the northwestern part of El-Missikat pluton (after Abu Dief, 1985), with locations of the studied profiles (red dashed lines)

silica veins was estimated at 27, 114, 390, 20, 43, 22, 226, and 231 reads. The obtained data set was then undergone statistically processing to study the varied correlations between them and drive the radio-elemental ratios,

including Th/U, U/K, and Th/K. On the other hand, the radioactive measurements were coupled by separation of radioactive minerals from some alteration zones and mineralized silica veins at El-Missikat and El-Erediya. For

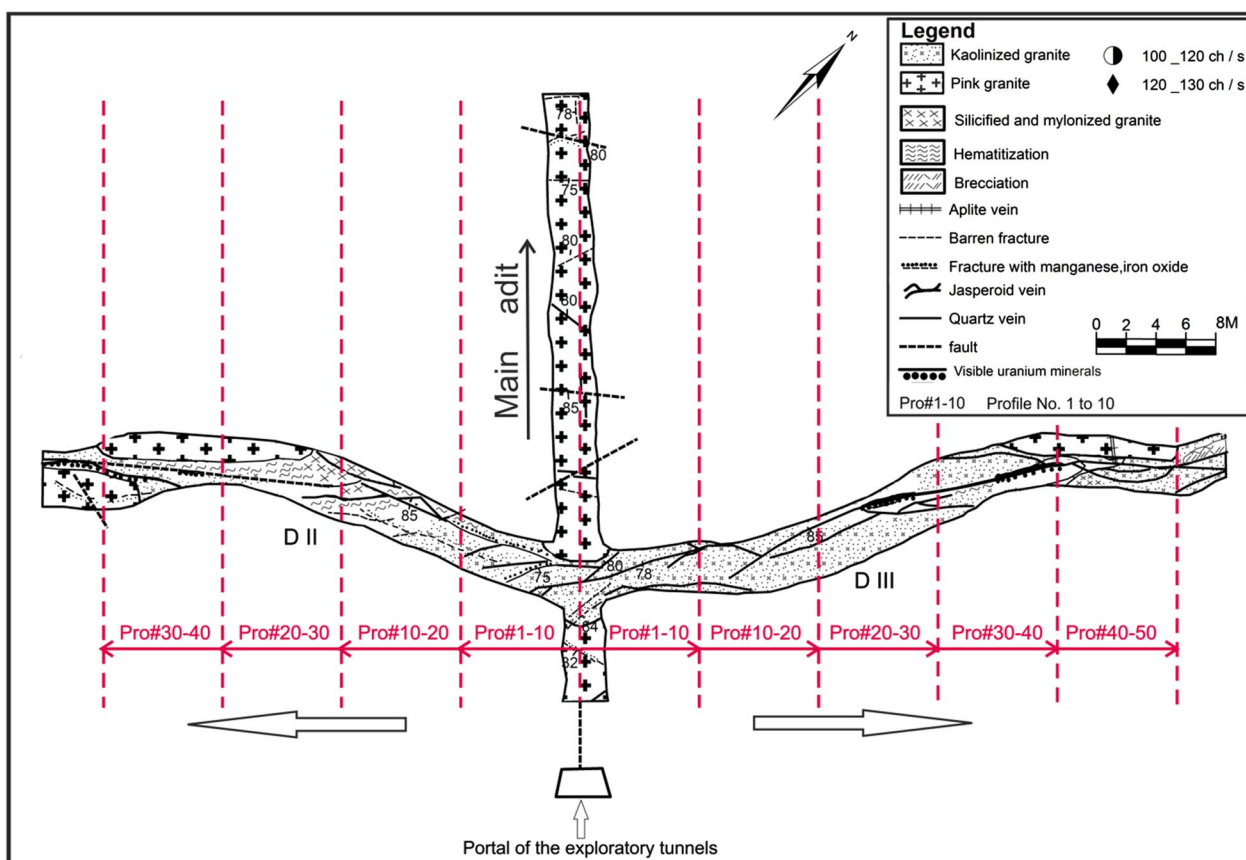


Fig. 3 Geological maps of drifts# DII&DIII through the southern part of El-Erediya pluton (after El-Tahir, 1985), with locations of the studied profiles (red dashed lines)

this purpose, representative samples were ground up to – 500 μm and then bromoform-based separation along with handpicking was conducted. The separated mineral fraction was investigated by SEM–EDX. Although the current approach depends mainly on the radiometric measurements, its validity can be substantiated by literature (e.g. Heikal et al. 2022) that compared the radioelemental ratios of the monzo-syenogranites (the Central Eastern Desert of Egypt) obtained by the ground-gamma ray spectrometer (e.g. avg. 2.53 Th/U ratio) in relative to the data obtained by ICP-MS (e.g. avg. 2.9 Th/U ratio).

Results and discussion

Distribution of radioelements through pink granites

As listed in Table 1, it is clear that the distribution of U, Th, and K through El-Missikat pink granite is greatly similar to El-Erediya counterpart. Comparing with the normal averages in granites (2–8 ppm U, 10–30 ppm Th, and 3.6–4.5% K) [44, 55, 60], El-Missikat (15.94 ppm U, 39.21 ppm Th, and 6.63% K) and El-Erediya pink granite (16.05 ppm U, 35.62 ppm Th, and 7.07% K) can be considered as anomalously radioactive rock suites. The

radioactivity is attributed mainly to the anomalous contents of U and Th due to the fact that K has radioactivity (e.g. 12–14 Ur) significantly lower than average granite (20 Ur) (Darnley, 1982). Th/U ratio is estimated at ranges of 1.30–3.5 (avg., 2.59) and 1.01–4.76 (avg., 2.42) for El-Missikat and El-Erediya pink granite, respectively. These values fall through the normal crustal ratio (2.5–5) [6, 21, 22], with some degree of U enrichment indicated by Th/U ratio below 2.5. Th/K ratio generally averages between 5.92×10^{-4} at El-Missikat and 5.05×10^{-4} at El-Erediya, and hence it can correspond to the normal crustal value of the unaltered lithologies, estimated at $5-3 \times 10^{-4}$ [38, 64]. However, Th enrichment can result in higher Th/K ratios than the normal range (e.g. 8.78 at El-Missikat and 6.37 at El-Erediya).

Distribution of radioelements through alteration zones

Altered granites are characterized by higher radio-measurements of U, Th, and K than that recorded for pink granite (Tables 2, 3). U has a general trend to be decreased from the brecciated granite (avg., 41.53–43.32 ppm at El-Missikat and 116.54–121.4 ppm at



Fig. 4 Field photographs show the alteration features of El-Missikat pink granite through DI and DII: **a** brecciation, **b** silicification, **c** greisenization, **d** hematitization, and **e** kaolinization



Fig. 5 Field photographs show the alteration features of El-Erediya pink granite through DII and DIII: **a** brecciation, **b** silicification, **c** jasperoid vein in silicified granite, and **d** kaolinization stained by hematitization



Fig. 6 Field photographs show the occurrence of yellowish-greenish yellow secondary U minerals, at DI of El-Missikat shear zone, as fracture infill hosted by the brecciated silica veins **a** and associated with fluorite (**b**-look at red arrow), with occasional occurrence through the kaolinized granite (**c**)

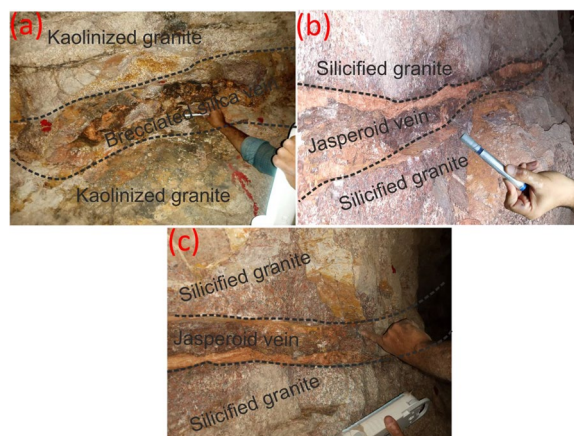


Fig. 7 Field photographs show mineralized silica veins stained by yellowish secondary uranium minerals at DII of El-Erediya shear zone: **a** brecciated silica vein and **b** and **c** jasperoid veins

El-Erediya), away from the center of shear zone, toward the kaolinized zone (avg., 29.73–29.84 ppm at El-Missikat and 35.79–49.54 ppm at El-Erediya). The latter is generally enriched in U compared to pink granite;

Table 1 Distribution of U, Th, and K in pink granite through the main adit at El-Missikat and El-Erediya exploratory tunnels

Lithology/Alterations	U (ppm)	Th (ppm)	K (%)	Th/U	(Th/K)*10 ⁻⁴	(U/K)*10 ⁻⁴
El-Missikat	Avg., 15.94	39.21	6.63	2.59	5.92	2.41
	Max., 35.0	59.7	7	3.3	8.78	5.16
	Min., 10.0	26	6	1.3	4.12	1.43
El-Erediya	Avg., 16.05	35.62	7.07	2.42	5.05	2.29
	Max., 39.1	42.7	8.5	4.76	6.37	5.75
	Min., 7.4	26.1	6	1.01	3.68	1.03

Table 2 Distribution of U, Th, and K for the different alteration zones through drift# D_I and D_{II} at El-Missikat exploratory tunnels

Lithology/alterations	U (ppm)	Th (ppm)	K (%)	Th/U	(Th/K)*10 ⁻⁴	(U/K)*10 ⁻⁴	
D _I	Brecciation	Avg., 43.32	58.93	4.57	1.4	15.19	11.17
		Max., 69.2	71.6	7.3	2.29	49	37
		Min., 29.2	48.2	1.2	0.76	7.65	4.29
	Silicification	Avg., 41.63	63.67	3.12	1.57	23.1	15.61
		Max., 59.1	71.9	6.7	2	31.38	26.86
		Min., 33.8	56.4	1.9	0.95	10.57	5.28
	Greisenization	Avg., 41.77	57.32	4.48	1.45	13.82	10.08
		Max., 71.9	72.5	6	2.46	38.33	23.33
		Min., 26.4	44.5	1.5	0.78	8.56	4.56
Kaolinization	Avg., 29.73	56.21	4.15	1.93	14.34	7.44	
	Max., 37.2	63.5	5.7	2.79	19.9	10.78	
	Min., 22.1	49.2	2.7	1.48	8.63	5.14	
D _{II}	Brecciation	Avg., 41.53	61.72	6.12	1.5	10.15	6.86
		Max., 45.0	72	7.6	1.79	12.82	8.42
		Min., 36.20	45.6	5.3	1.01	7.35	5.04
	Greisenization	Avg., 36.11	56.4	4.46	1.64	14.34	9.38
		Max., 95.6	70.2	6.9	3.03	89.86	65
		Min., 19.0	36.3	0.7	0.6	8.05	4.45
	Kaolinization	Avg., 29.84	54.89	4.9	1.87	11.57	6.32
		Max., 37.2	63	6.1	2.72	17.11	10.69
		Min., 23.2	45.4	3.2	1.4	8.05	4.62

Table 3 Distribution of U, Th, and K for the different alteration zones through drift# D_{II} and D_{III} at El-Erediya exploratory tunnels

Lithology/Alterations	U (ppm)	Th (ppm)	K (%)	Th/U	(Th/K)*10 ⁻⁴	(U/K)*10 ⁻⁴	
D _{II}	Brecciation	Avg., 121.4	32	6.01	0.35	5.38	21.49
		Max., 161.3	32.8	7.3	0.65	6.39	31.63
		Min., 47.2	30.6	5.1	0.2	4.19	6.47
	Hematitization	Avg., 110.84	33.24	6.91	0.37	4.85	16.14
		Max., 266.1	41.8	8.2	0.67	6.47	32.45
		Min., 49.7	26.6	5.9	0.13	3.8	6.37
	Kaolinization	Avg., 35.79	35.69	6.78	1.12	5.83	5.71
		Max., 89.2	102.5	8.3	2.91	51.25	29.7
		Min., 12.9	26.5	2	0.34	3.61	1.7
D _{III}	Brecciation	Avg., 116.54	39.44	6.56	0.38	6.04	17.78
		Max., 184.6	58.7	7.2	0.56	8.27	26.75
		Min., 61.6	29.3	5.3	0.16	4.25	9.78
	Hematitization	Avg., 124.01	35.46	6.29	0.3	5.76	20.04
		Max., 184.6	43.8	7.1	0.42	7.08	26.75
		Min., 66.0	23.2	4.8	0.16	3.27	9.3
	Kaolinization	Avg., 49.54	42.17	4.67	0.9	12.39	13.48
		Max., 95.8	219.5	8.5	7.42	199.5	41.14
		Min., 19.3	16.3	0.8	0.38	3.88	2.74

Table 4 Distribution of U, Th, and K through U-mineralized silica veins at El-Missikat and El-Erediya exploratory tunnels

Lithology/alterations	U (ppm)	Th (ppm)	K (%)	Th/U	(Th/K)*10 ⁻⁴	(U/K)*10 ⁻⁴
Drift# D _I						
El-Missikat tunnels						
Massive silica veins	Avg., 82.19	56.12	3.04	1.02	23.5	37.6
	Max., 676	76.2	6.3	2.11	195.33	200
	Min., 26.1	42.2	0.3	0.11	10.33	6.07
Brecciated silica veins	Avg., 121.1	54.65	3.07	0.86	20.37	41.44
	Max., 1007.7	78.8	6.4	1.81	68.6	185
	Min., 29.2	35.3	1	0.08	9.38	5.54
Drift# D _{II}						
Massive silica veins	Avg., 54.66	51.81	4.34	1.13	12.53	51.06
	Max., 224.2	67.2	6.7	2.21	25.64	521.71
	Min., 23.4	38	2.5	0.22	7.68	6.65
Brecciated silica veins	Avg., 88.16	53.74	2.62	0.82	27.65	13.62
	Max., 487.0	72.1	5.6	1.71	120.8	89.68
	Min., 66.0	23.2	4.8	0.16	3.27	5.13
El-Erediya tunnels						
Drift# D _{II}						
Red silica veins	Avg., 183.26	37.78	6.43	0.33	6.68	29.7
	Max., 536.4	95.2	9.8	1.35	36.62	92.48
	Min., 49.2	24.7	2.6	0.07	4.12	7.45
Drift# D _{III}						
Red silica veins	Avg., 312.65	92.22	9.86	0.63	12.76	30.67
	Max., 2990.5	685.8	84.4	2.24	56.04	159.81
	Min., 41.5	23.5	2.4	0.06	4.37	8.56

however, the low surface area of kaolinite limits the number of adsorption sites for U⁺⁶ ions carried by the invading solutions [69]. This can interpret the lower U values of the kaolinized granite compared to the other alteration zones, including brecciation (avg., 41.53–43.32 ppm at El-Missikat and 116.54–121.4 ppm at El-Erediya), silicification (avg., 41.63 ppm at El-Missikat), greisenization (avg., 36.11–41.77 ppm at El-Missikat), and hematitization (avg., 110.84–124.01 ppm at El-Erediya). Also, the maximum U values are measured from greisenization at El-Missikat (71.9–95.6 ppm) and hematitization at El-Erediya (184.6–266.1 ppm), complying with the hypothesis that greisenized and hematitic alterations are among the favorable environments for U accommodation (e.g. [19, 25]).

Th is measured through the alteration zones of El-Missikat at averages of 58.93–61.72 ppm, 63.67 ppm, 56.4–57.32 ppm, and 54.89–56.21 ppm corresponding to brecciation, silicification, greisenization, and kaolinization, respectively. Comparing with pink granite (avg., 39.21 ppm), there is a noticeable Th enrichment illustrated by Th/U > 1. Depending on the low mobilization behavior of Th in both the hypogene and

supergene fluids [54], successive pulses of mineralized solutions are expected. On the other hand, Th values through El-Erediya alteration zones generally exhibit slight depletion (e.g. avg., 33.24–35.46 ppm for hematitization) in relative to pink granite (avg., 35.62 ppm) and the higher U enrichment, resulting in Th/U < 1. For K, its average values remarkably decline (e.g. brecciation “4.56–6.12%”, silicification “3.12%”, greisenization “4.46–4.48%”, and kaolinization “4.15–4.90%”) away from that measured for pink granite at El-Missikat (avg., 6.63%), indicating moderately altered K-feldspar was imposed. Except for kaolinization (avg., 4.56%) through D_{III} at El-Erediya, slight changes of K contents (e.g. avg., 6.01–6.78%) in relative to pink granite (avg., 7.07%) are perceived. All of these changes in K contents are reflected by fluctuations of Th/K ratio above and below the normal value 5*10⁻⁴.

Distribution of radioelements through silica veins

Through El-Missikat shear zone (Table 4), U contents in brecciated silica veins (e.g. avg., 88–121 ppm and max., 487–1007.7 ppm) are remarkably higher than the massive veins (e.g. avg., 54.66–82.19 ppm and max.,

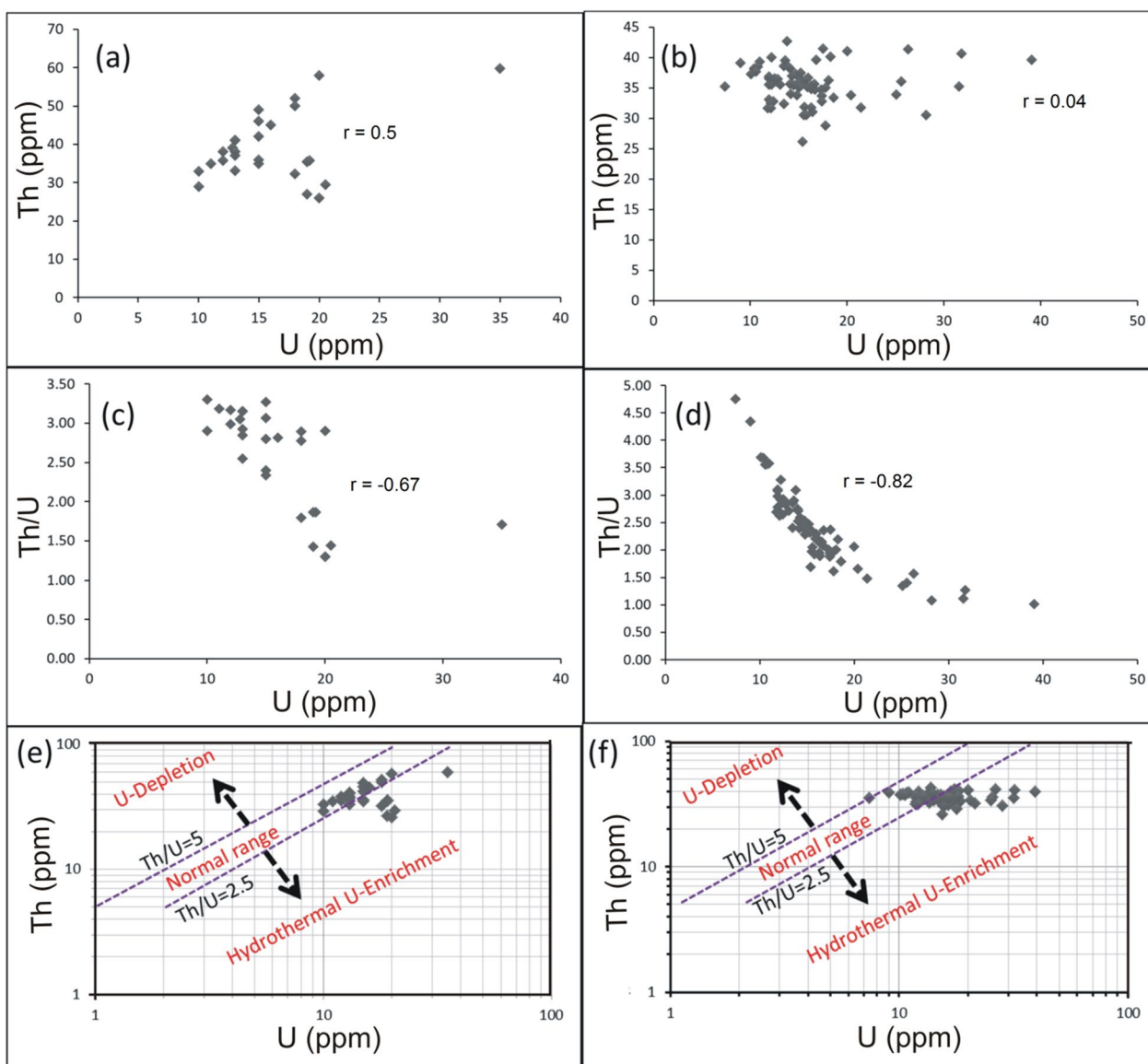


Fig. 8 Binary plot of Th and Th/U ratio vs. U for El-Missikat **a** and **c** and El-Erediya pink granite **b** and **d**, along with variation diagrams (e- El-Missikat and f- El-Erediya) of Th/U ratio showing that the granite-contained U is of both magmatic (2.5–5 Th/U ratio) and hydrothermal sources (Th/U<2.5)

224.2–676 ppm), indicating other pulses of U-bearing hydrothermal solutions emplaced due to the reactivation of shear zone that in turn caused brecciation of the early-formed silica veins. On the other side, the red silica veins at El-Erediya are characterized by the highest U anomalies (e.g. avg., 183.26–312.65 ppm and max., 536.4–2990.5 ppm), probably due to the co-occurrence of silica and iron oxyhydroxides. The former is considered as a favorable repository for U accommodation that is facilitated by the latter whose task is to adsorb and reduce the dissolved U^{+6} ions [50].

Genetic implications using Th/U ratio

U and Th are incompatible trace elements mostly concentrated in granitic magmas where they behave, without fractionation, as tetravalent ions related to each other. This relation is expressed as Th/U ratio that normally varies between 2.5 and 5 [6]. For the felsic magmatism, Th/U ratio is considered as a good indication for the magmatic differentiation degree between peralkaline and peraluminous granitic suites. In peralkaline magma the excess of alkalis in relative to alumina and the high temperature conditions induce high solubility of Th and U-bearing

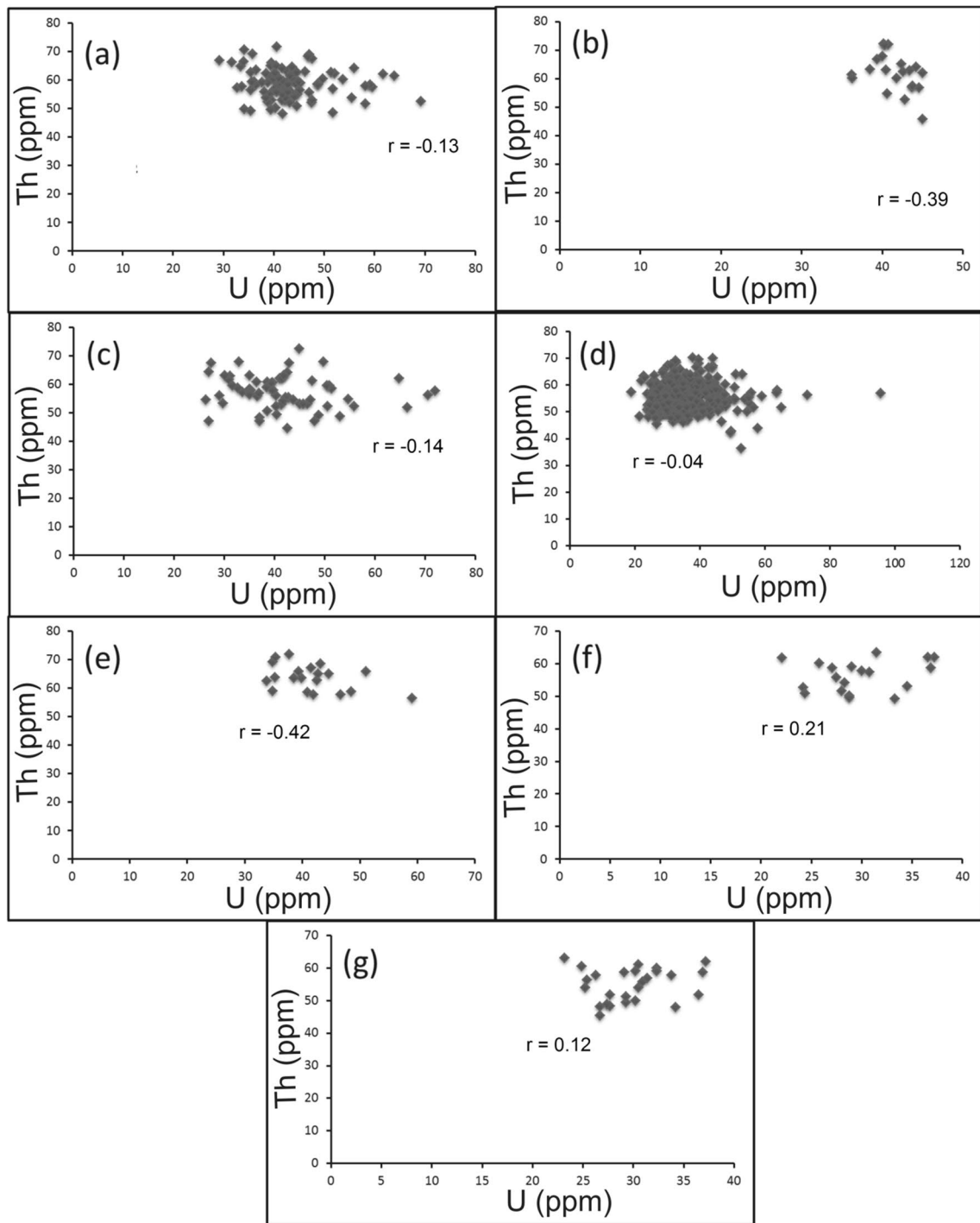


Fig. 9 Binary plot of Th vs. U through the different alteration zones at El-Missikat drifts# DI **a**, **c**, **e**, and **f** assigned to brecciation, greisenization, silicification, and kaolinization) and DII (**b**, **d**, and **g** assigned to brecciation, greisenization, and kaolinization) showing weak correlation coefficients as an indication for U-enrichment

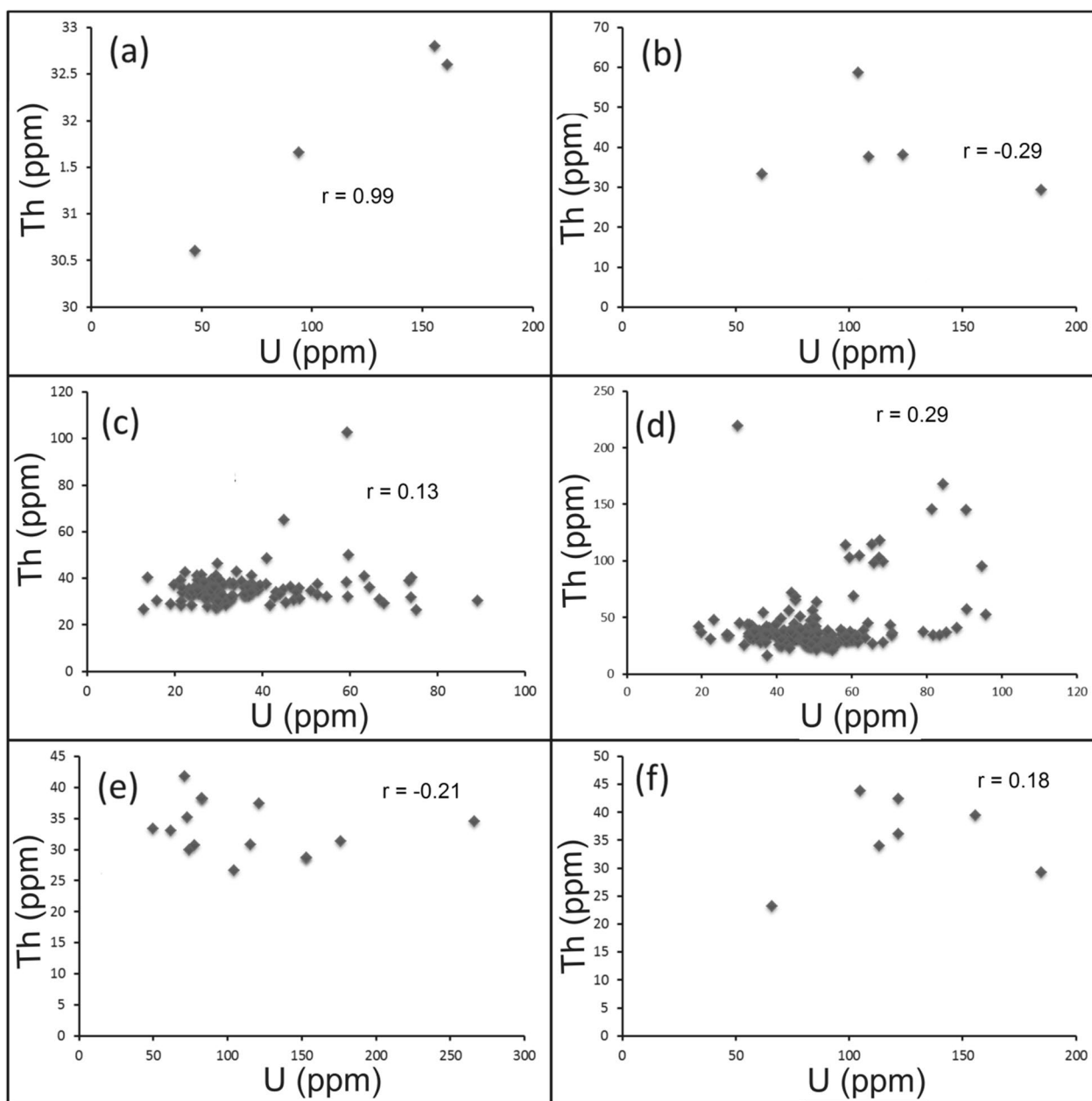


Fig. 10 Binary plot of Th vs. U through the different alteration zones at El-Erediya drifts# DII **a, c,** and **e** assigned to brecciation, kaolinization, and hematitization) and DIII **b, d,** and **f** assigned to the same order) showing weak correlation coefficients as an indication for U-enrichment

accessory minerals. Hence, the two elements are concentrated with each other and their Th/U ratio remains close to the average crustal ratio ~ 4 . On the other side, the per-aluminous conditions favor low solubility and fractionation of Th-bearing accessory minerals (e.g. monazite), resulting in an increase of U contents and Th/U ratios < 4

[23]. In all cases, Th and U contents of magmatic origin reveal a strong positive correlation. Comparing with the current study, pink granites of El-Missikat (Fig. 8a) and El-Erediya (Fig. 8b) exhibit moderate and very weak relationship between Th and U at correlation coefficients of 0.5 and 0.04, respectively, indicating U enrichment.

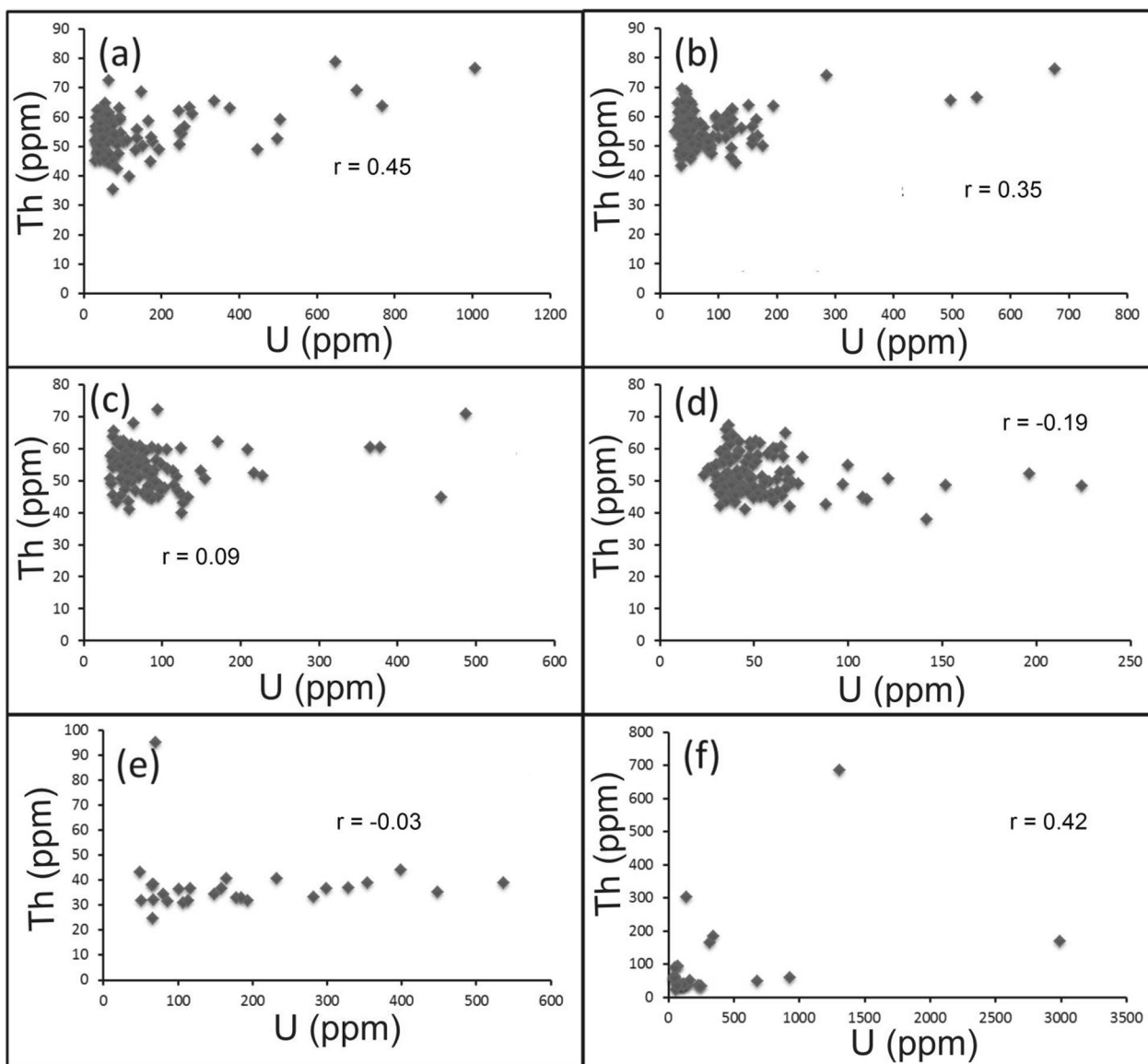


Fig. 11 Binary plot of Th vs. U through varied siliceous veins at El-Missikat (a and b brecciated and massive silica veins through drift#DI and c and d brecciated and massive silica veins through drift#DII) and El-Erediya (e & f reddish silica veins through drifts# DII and DIII)

Also, U contents exhibit a strong negative correlation with Th/U ratios for El-Missikat ($r = -0.67$) (Fig. 8c) and El-Erediya pink granite ($r = -0.82$) (Fig. 8d). Further, the calculated Th/U ratios fall through the normal range and below 2.5. Accordingly, magmatic and post-magmatic origin can be presumed for the granite-hosted U mineralization. The post-magmatic source can be either hydrothermal or supergene solutions. The former can be discriminated from the latter using Th/U ratio

whose range “ $2.5 > Th/U > 0.1$ ” is assigned to the hydrothermal uranium mineralizations [17, 40, 68], while values ≤ 0.1 are associated with supergene enrichment [15, 16]. These values, along with the normal ratio, are collectively represented by Th-U variation diagram on which both magmatic and hydrothermal sources are assigned to the anomalous radioactivity of the studied granite at El-Missikat (Fig. 8e) and El-Erediya (Fig. 8f). Another clue can be driven from Th/U ratios measured by Mohammed

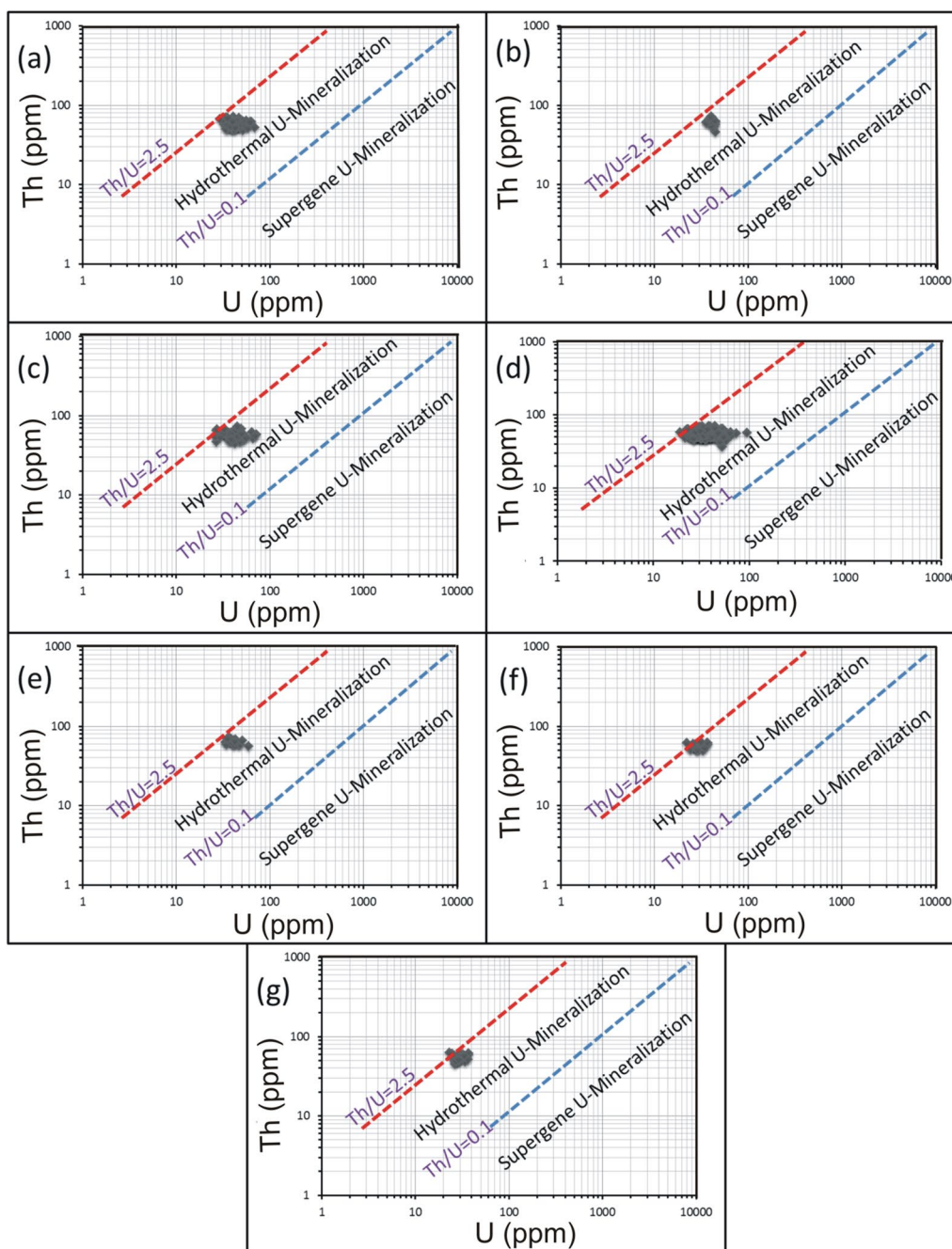


Fig. 12 Th-U variation diagrams of EI-Missikat alteration zones at drifts#DI (a, c, e, and f assigned to brecciation, greisenization, silicification, and kaolinization) and DI1 (b, d, and g assigned to brecciation, greisenization, and kaolinization) discriminate between hydrothermal ($2.5 > Th/U > 0.1$) and supergene U-mineralization (Th/U ratios ≤ 0.1)

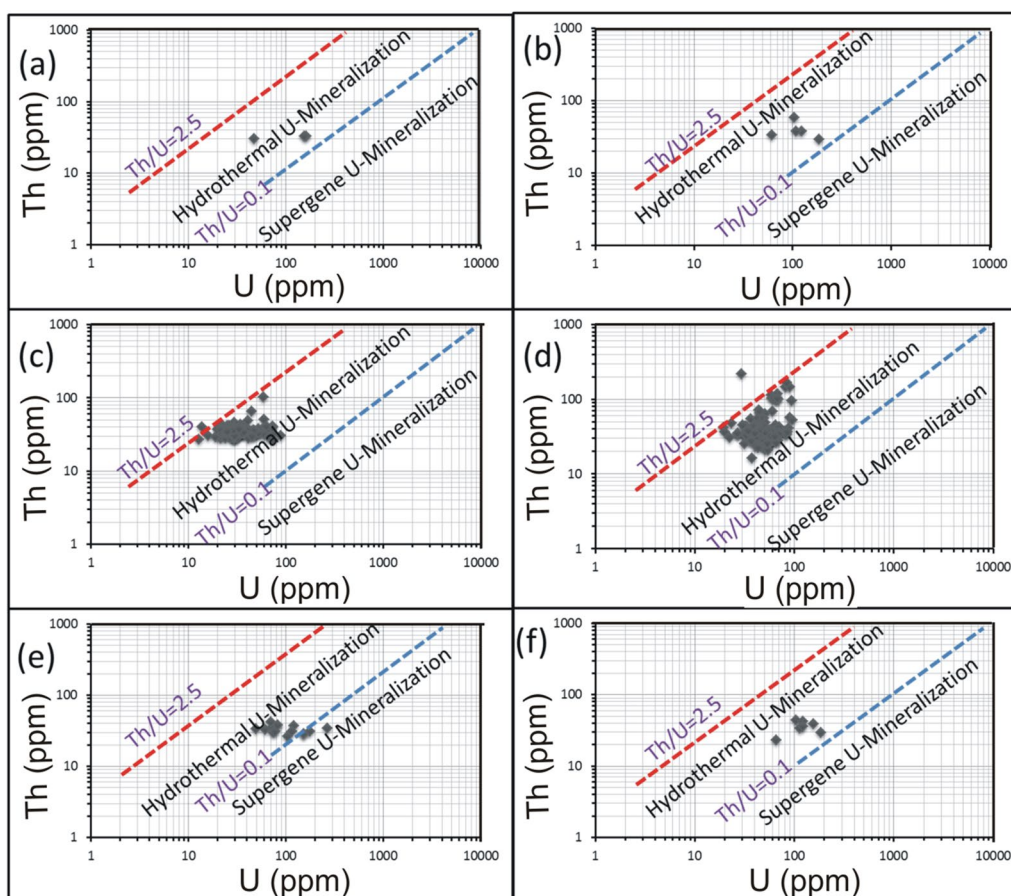


Fig. 13 Th-U variation diagrams of El-Erediya alteration zones at drifts# DII (a, c, and e assigned to brecciation, kaolinization, and hematitization) and DIII (b, d, and f assigned to the same order) discriminate between hydrothermal ($2.5 > \text{Th}/\text{U} > 0.1$) and supergene U-mineralization ($\text{Th}/\text{U} \leq 0.1$)

[52] for zircon crystals separated from El-Missikat “0.24” and El-Erediya granite “0.30”. Discussion of these values here according to the recent works (e.g. [45, 61, 70, 71] that categorized zircon into magmatic “ $\text{Th}/\text{U} > 0.5$ ”, hydrothermal “ $0.5 > \text{Th}/\text{U} \leq 0.1$ ”, and metamorphic variety “ $\text{Th}/\text{U} \leq 0.1$ ”, supports the aforementioned hydrothermal origin.

For alteration zones and mineralized silica veins, U enrichment is also reflected by the weak correlation between Th and U (Figs. 9, 10, 11). On Th-U variation diagram, most of the data are concentrated through the hydrothermal field, with an exception for the brecciated silica veins at El-Missikat as well as red silica veins and hematitization at El-Erediya where some samples fall through the field of supergene enrichment (Figs. 12,

13, 14). Besides radiometric measurements, the mineral separation for the highly anomalous, mineralized-vein samples revealed the occurrence of some hydrothermally sourced, radioactive minerals, including thorite, betafite, coffinite, and zircon, and some supergene U minerals represented mainly by uranophane and kasolite (Table 5). The aforementioned hydrothermal minerals probably refer to the magmatic source of some pluses of the invading hydrothermal solutions. This claim is suggested according to a number of facts, including the concentration of Th in the residual magmatic fluids, the occurrence of Th-rich minerals (e.g. thorite, and zircon), and the poor liberation behavior of Th from its host rocks by hydrothermal solutions.

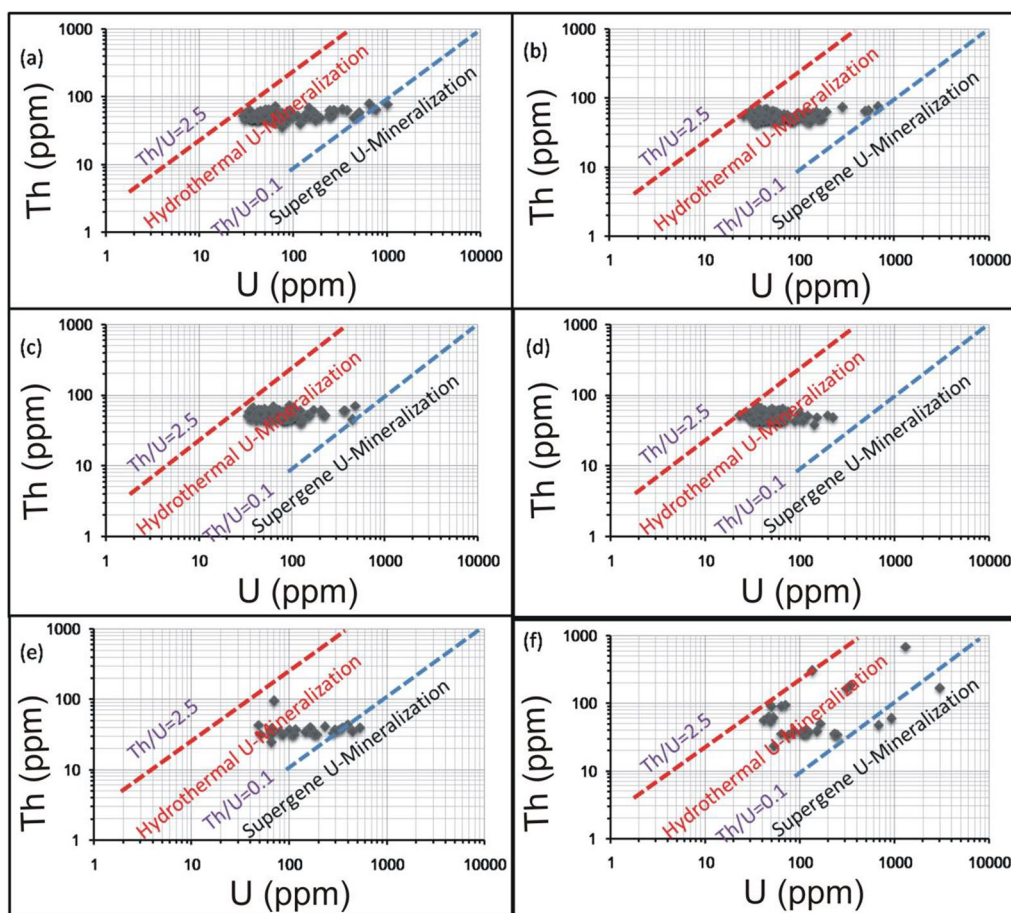


Fig. 14 Th-U variation diagrams of the mineralized silica veins at El-Missikat (**a** and **b** brecciated and massive silica veins through drift#DI and **c** and **d** brecciated and massive silica veins through drift#DII) and El-Erediya (**e** and **f** reddish silica veins through drifts# DII and DIII) discriminate between hydrothermal ($2.5 > \text{Th}/\text{U} > 0.1$) and supergene U-mineralization (Th/U ratios ≤ 0.1)

Genetic implications using Th/K ratio

Th and K are concentrated during the late stages of magmatic differentiation, resulting in a strong positive correlation and $3\text{--}5 \cdot 10^{-4}$ Th/K ratios for the unaltered rocks [38, 64]. Through this context, Th values were plotted against K contents for the pink granite at El-Missikat and El-Erediya (Fig. 15a and b). This binary plot shows that the two elements are not related to each other ($r=0.14$ and 0.15 for El-Missikat and El-Erediya, respectively), implying that the studied granite experienced either Th enrichment or K-metasomatism (potassic alteration). By using Th-K variation diagram constructed from the aforementioned normal ratios, the plotted samples of El-Missikat (Fig. 15c) and El-Erediya (Fig. 15d) pink granite are located through the normal range and the field of Th enrichment in which Th/K ratio $> 5 \cdot 10^{-4}$, while no samples are found through the field of K-metasomatism where $\text{Th}/\text{K} < 3 \cdot 10^{-4}$. For shear zone, Th-enrichment is considered to be the

dominant feature through El-Missikat alteration zones, including brecciation (Fig. 16a and b), greisenization (Fig. 16c and d), silicification (Fig. 16e), and kaolinization (Fig. 16f and g). On the other side, El-Erediya shear zone is characterized by the occurrence of Th enrichment along with normal Th/K ratio through the different alteration features, comprising brecciation (Fig. 17a and b), kaolinization (Fig. 17c and d), and hematitization (Fig. 17e and f). It is worth to mention that the occurrence of normal Th/K ratio through El-Erediya alteration zones likely indicates some pulses of the hydrothermal solutions caused K-metasomatism. Another genetic implication of Th/K ratio is revealed here by its relationship with U/K ratio. It was found that Th/K ratio has a strong positive correlation with U/K ratio through the studied alteration zones (Figs. 18, 19) where thorite, zircon, betafite, and coffinite are common. On the other hand, hematitization, red and brecciated silica veins exhibit weak correlations

Table 5 EDX analysis of the separated radioactive minerals from some altered granites and silica veins at El-Missikat and El-Erediya exploratory tunnels

Elements %	Thorite		Betalite		Zircon		Coffinite		Uranophane		Kasolite
	A	B	C	D	E	F	G	H	I	J	K
SiO ₂	34.82	28.30	–	–	45.9	42.2	25.2	23.8	38.9	53.92	43.88
UO ₂	8.55	10.90	36.9	28.7	4.2	3.4	65.8	67.2	53.7	33.73	30.03
ThO ₂	42.29	49.12	1.22	2.4	1.07	1.3	–	–	–	–	–
Al ₂ O ₃	2.77	1.97	5.77	3.45	7.30	6.2	0.65	0.12	3.67	5.08	4.8
TiO ₂	–	–	25.5	29.2	–	–	–	–	–	–	–
CaO	–	0.42	1.4	1.08	1.95	2.7	1.2	2.5	1.0	1.97	–
PbO	–	0.30	–	0.10	–	–	2.3	2.51	0.1	0.2	20.17
FeO	2.98	0.25	2.35	2.16	1.58	–	0.9	1.7	1.5	4.32	–
BaO	–	–	0.08	0.48	–	–	0.5	0.9	–	–	–
ZrO ₂	–	–	–	–	30.9	35.5	–	–	0.1	0.4	–
Nd ₂ O ₃	–	–	2.5	3.7	–	–	0.14	0.11	–	–	–
Y ₂ O ₃	7.59	8.23	0.89	0.45	5.78	6.0	1.05	0.83	–	–	–
Ce ₂ O ₃	–	–	1.53	2.78	–	–	0.29	0.28	–	–	–
Ta ₂ O ₅	–	–	3.41	4.51	–	–	–	–	–	–	–
Nb ₂ O ₅	–	–	16.6	20.7	–	–	–	–	–	–	–
Total	99.0	99.49	98.2	99.7	98.6	97.3	98.03	99.9	98.97	99.62	98.88

* A—Greisenization through DII of El-Missikat; B—Kaolinization through DIII of El-Erediya; C—red silica veins through DII of El-Erediya; D—brecciated silica veins through DI of El-Missikat; E—silicification through DI of El-Missikat; F—brecciated granite through DII of El-Erediya; G and H—massive and brecciated silica veins, respectively, through DII of El-Missikat; I and J—hematization and red silica veins, respectively, through DIII of El-Erediya; K—brecciated silica veins through DII of El-Missikat

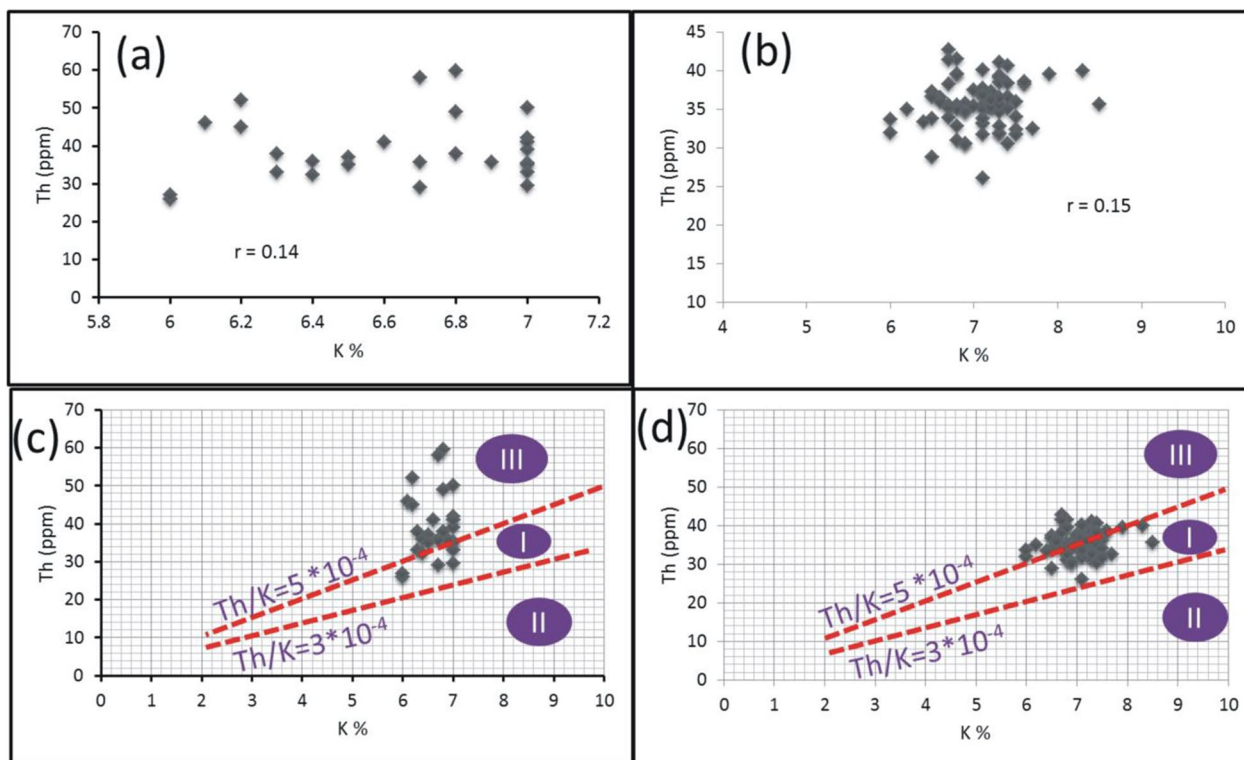


Fig. 15 Th-K binary plot shows weak correlations of El-Missikat **a** and El-Erediya pink granite **b**, along with Th-K variation diagrams reveal normal Th/K ratio (I) ($3-5 \times 10^{-4}$) and Th-enrichment (III) ($Th/K > 5 \times 10^{-4}$) of El-Missikat **c** and El-Erediya pink granite **d**, without any signs for K-metasomatism (II) ($Th/K < 3 \times 10^{-4}$)

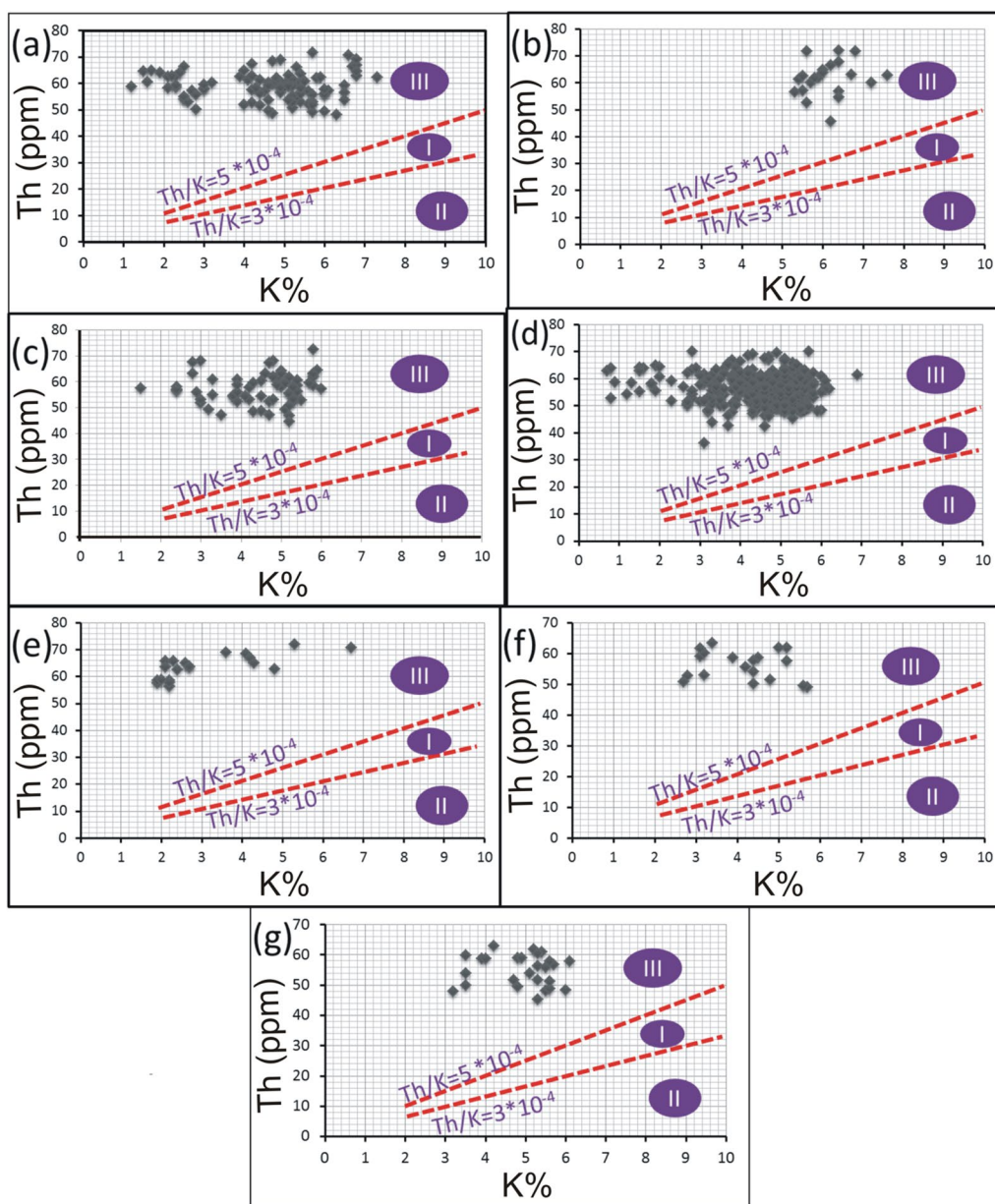


Fig. 16 Th-K variation diagrams indicate the dominance of Th-enrichment (III) through the alteration zones of El-Missikat exploratory tunnels (a and b brecciation, c and d greisenization, e silicification, f and g kaolinization)

(Fig. 20) and characterized by the abundance of secondary uranium minerals (e.g. uranophane and kasolite). K values are the same for the two ratios, so the strength of correlation indicate the extent to which U and Th mineralizations are associated with each other. In contrast to U, the weak mobilization of Th in supergene solutions causes much lower concentrations [60], and hence there is no chance to correlate with U. On the other side, hydrothermal U mineralization can be associated with hydrothermal Th mineralization (e.g.

magmatic-hydrothermal solutions). At this point, it is claimed that Th/K vs. U/K can be used to discriminate between hydrothermal (strong positive correlation) and supergene uranium mineralizations (weak correlation).

Conclusion

The detailed study of distribution of U, Th, and K as well as their ratios (Th/U, U/K, and Th/K ratios) through U mineralizations has proven its vital role in providing sufficient information to build-up a genetic scenario about

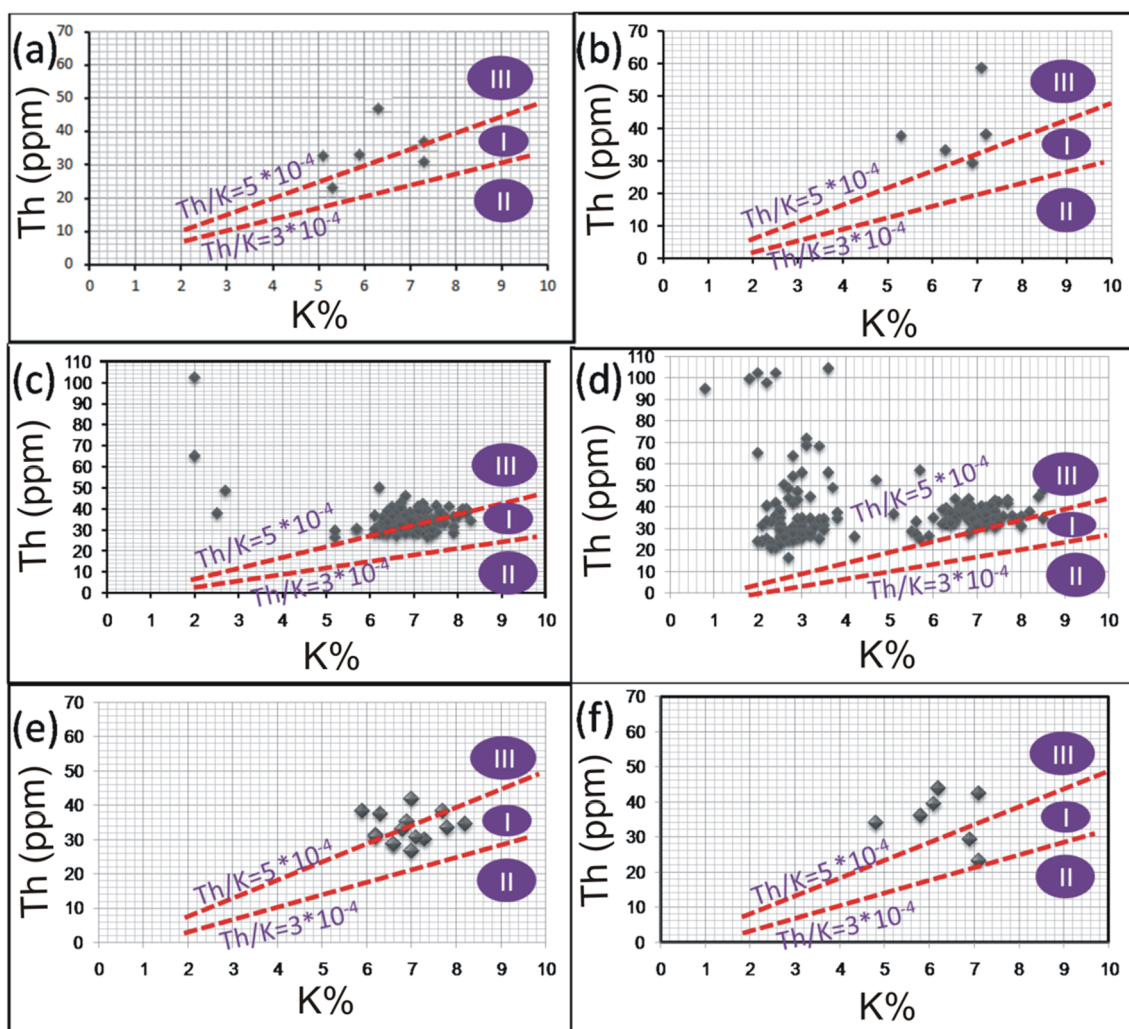


Fig. 17 Th-K variation diagrams show that most measurements through El-Erediya alteration zone (a and b brecciation, c and d kaolinization, e and f hematization) fall through the normal range (I) and Th-enrichment (III)

magmatic, hydrothermal, and supergene U deposits. This was manifested by considering the shear zone-related U mineralizations through El-Missikat and El-Erediya exploratory tunnels, the Central Eastern Desert of Egypt, as a case study, where varied alteration zones, primary and secondary U mineralizations are well-exposed. Accordingly, our radiogenic ratios-based genetic scenario can be summarized through three main steps:

- (1) Tectonic shearing of the pink granite where many pathways become available for the upcoming mineralized solutions.
- (2) Many successive pulses of U and Th-bearing hydrothermal solutions, some of which are magmatic in origin, invaded the sheared granite and inferred by

the weak correlation between U and Th (e.g. $r=0.5$ and 0.04 for El-Missikat and El-Erediya granites, respectively) as well as Th and K (e.g. $r=0.14$), $2.5 > Th/U > 0.1$, $Th/K > 5 \cdot 10^{-4}$, the occurrence of thorite, columbite, xenotime and hydrothermal zircon ($0.5 > Th/U \leq 0.1$), and the strong positive correlation between Th/K and U/K ratios (e.g. $r=0.74$ and 0.80 in greisenized and kaolinized granite at El-Missikat and El-Erediya, respectively).

- (3) The hydrothermal U mineralization was then affected by the action of chemical weathering, resulting in the occurrence of secondary U minerals, including uranophane, kasolite, and zippeite, in places nearby the shear zone (e.g. brecciated

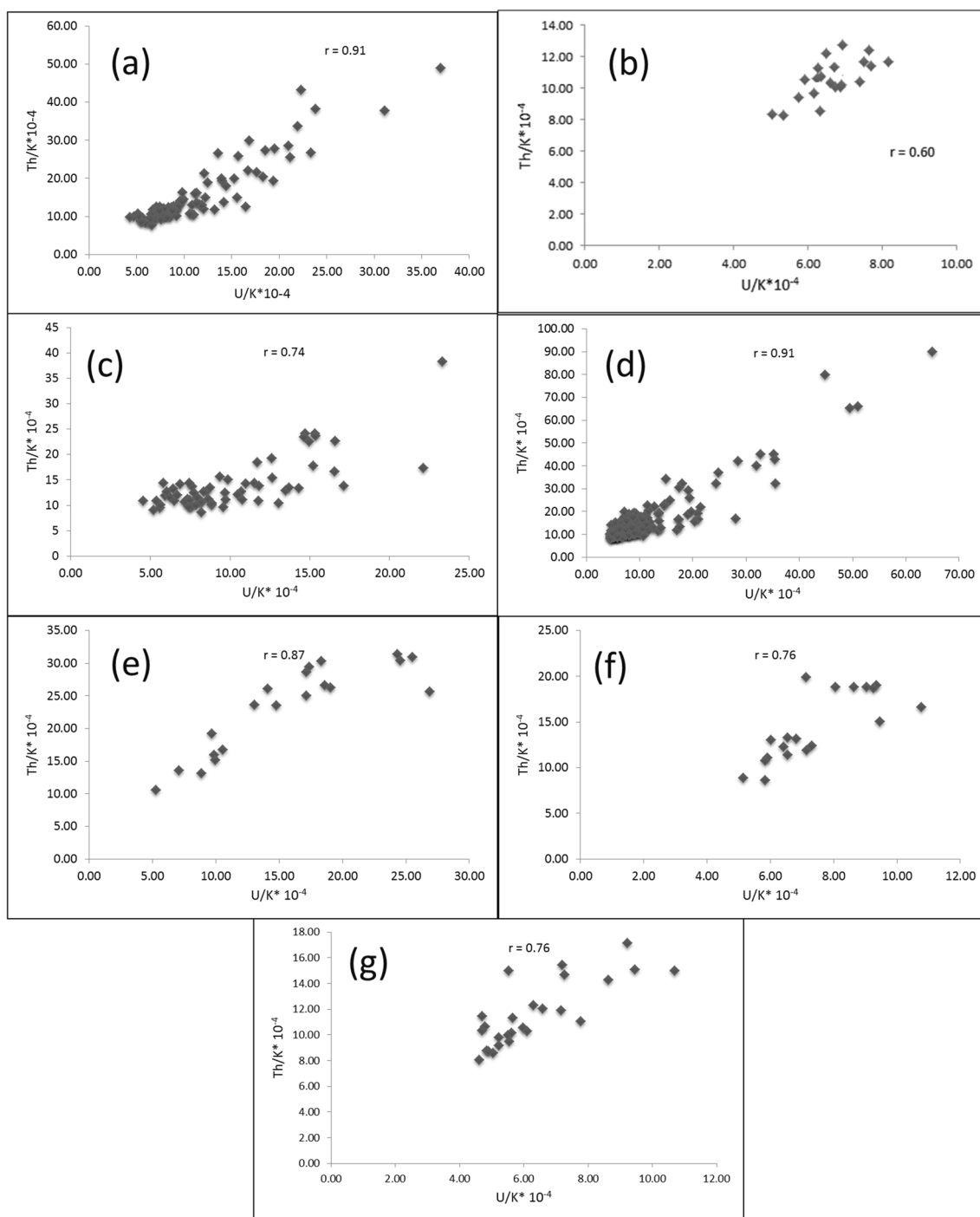


Fig. 18 Binary plot of Th/K vs. U/K ratios showing strong positive correlations through the alteration zones of El-Missikat exploratory tunnels (**a** and **b**-brecciation, **c** and **d**-greisenization, **e**-silicification, and **f** and **g**-kaolinitization)

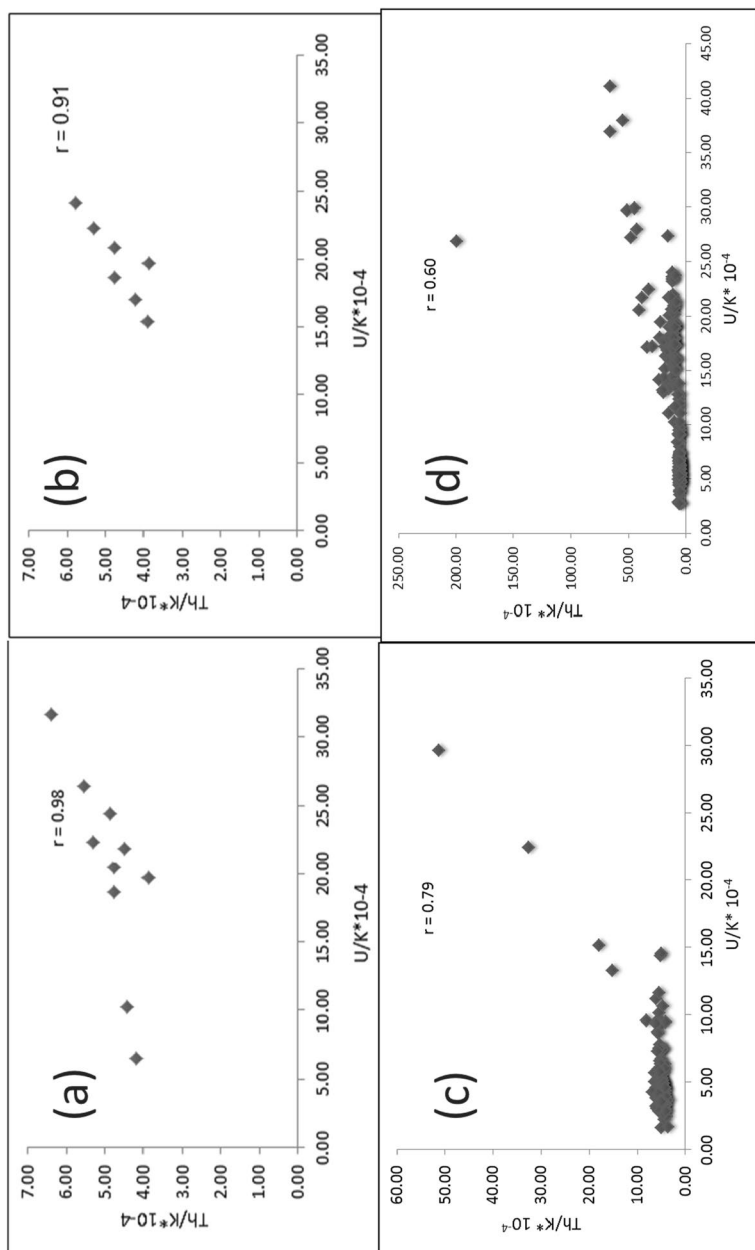


Fig. 19 Binary plot of Th/K vs. U/K ratios showing strong positive correlations through the alteration zones of El-Frediya exploratory tunnels (a and b-brecciation and c&d-kaolinization)

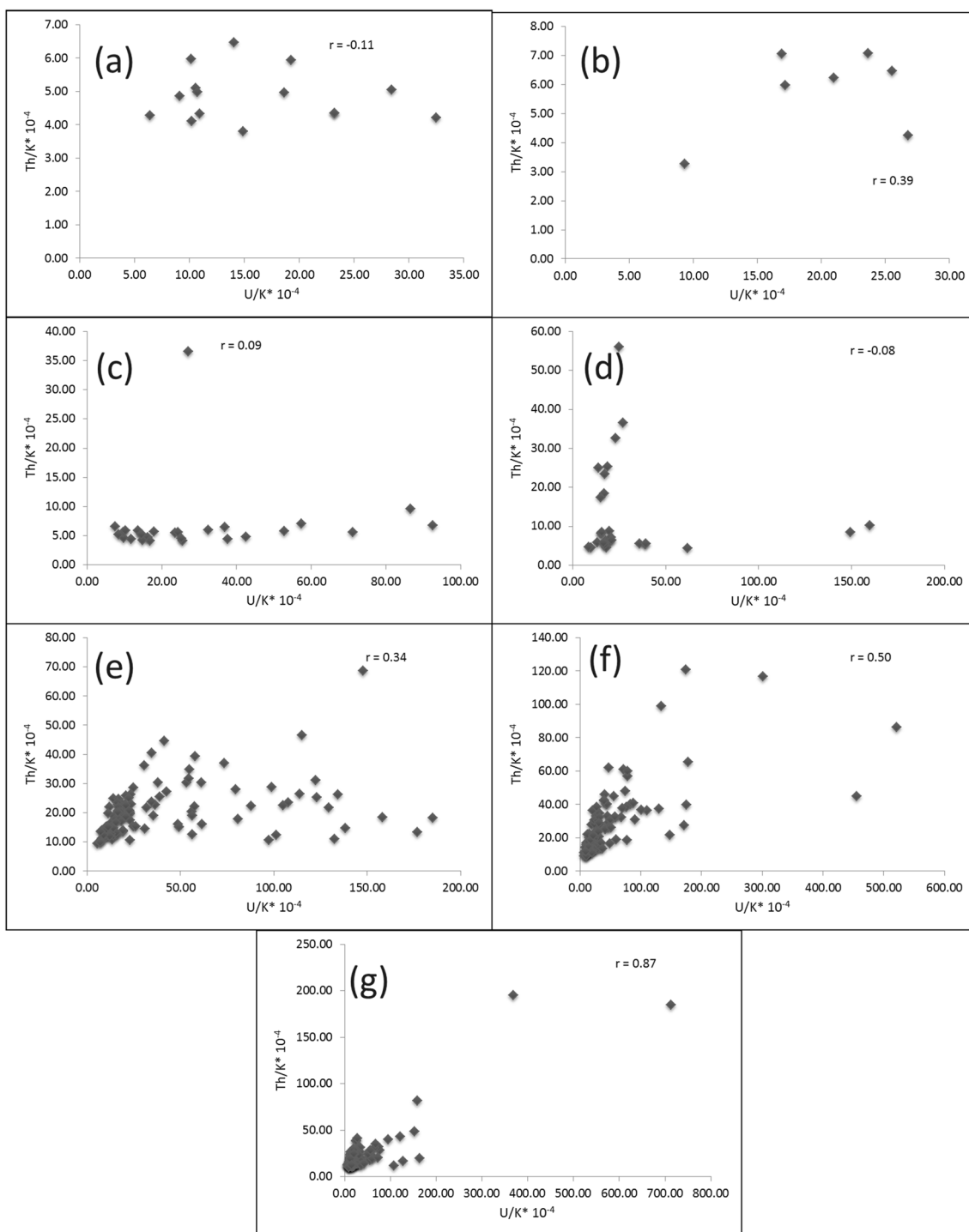


Fig. 20 Binary plot of Th/K vs. U/K ratio showing weak correlations through hematitization (a and b-El-Erediya), red silica veins (c and d-El-Erediya), brecciated silica veins (e and f-El-Missikat), and massive silica veins (g-El-Missikat)

and red silica veins and brecciated granite) where the supergene solutions readily percolate. This is reflected mainly by Th/U ratios ≤ 0.1 and the weak correlation between Th/K and U/K ratios (e.g. $r = 0.34$ and 0.08 for brecciated and red silica veins, respectively).

Acknowledgements

Authors are so grateful and highly appreciate the great collaboration made by the Egyptian Nuclear Materials Authority during field trips and sample collection.

Author contributions

The current topic was suggested by Dr. Abdel-Hakeem and Dr. Tahir; Field works and data collection were carried out by Dr. Abdel-Hakeem, Dr. Tahir, and Dr. Rageh; Data interpretation and manuscript writing were performed by Dr. Ehab and Dr. Abdel-Hakeem.

Funding

Open access funding provided by The Science, Technology & Innovation Funding Authority (STDF) in cooperation with The Egyptian Knowledge Bank (EKB). There is no funding for the current work.

Availability of data and materials

All data are represented here.

Declarations

Competing Interests

The authors declare that they have no known competing financial interests or personal relationships that could have appeared to influence the work reported in this paper.

Received: 31 July 2023 Accepted: 9 October 2023

Published online: 17 October 2023

References

- Abdel Hamid AA, El Sundoly HI, Abu Steet AA (2018) Hydrothermal alteration and evolution of Zr-Th-U-REE mineralization in the micro-granite of Wadi Ras Abda, North Eastern Desert. *Egypt Arabian J Geosci* 11(273):1–15
- Abu Dief A (1993) The relation between the uranium mineralization and tectonics in some Pan-African granite, west of Safaga, Eastern Desert, Egypt, Ph.D. Thesis. Assuit University.
- Abu-Deif A (1985) Geology of Uranium Mineralization in El-Missikat Area, Qena-Safaga Road, Eastern Desert, Egypt, M. Sc. Thesis, Al-Azhar Univ, Cairo: 103 p.
- Abu-Deif AA, El-Tahir MA (2008) A new uranium occurrence, Gabal El-Missikat Prospect, Central Eastern Desert. *Egypt Earth Sciences* 19(1):85–97
- Abu-Deif A, Abouelnaga HS, Hassanein HI (2001) Distribution of radioelements and its relation to uranium migration, El Erediya exploratory tunnels, central Eastern Desert. *Egypt J King Abdulaziz Univ (Earth Sci)* 13:19–40
- Allégre CJ, Dupré B, Lewin E (1986) Thorium/Uranium Ratio of the Earth. *Chem Geol* 56:219–227
- Ammar A A (1973) Application of aerial radiometry to the study of the geology of Wadi El-Gidami, Eastern Desert (with aeromagnetic application), Ph.D. Thesis, Faculty of Science, Cairo University, 424. P.
- Artemieva IM, Thybo H, Jakobsen K, Sørensen NK, Nielsen LSK (2017) Heat production in granitic rocks: Global analysis based on a new data compilation GRANITE2017. *Earth Sci Rev* 172:1–26
- Awad HA, Zakaly HM, Nastavkin AV, El Tohamy AM, El-Taher A (2021) Radioactive mineralizations on granitic rocks and silica veins on shear zone of El-Missikat area, Central Eastern Desert. *Egypt Appl Radiation Isotopes* 168:109493
- Bakhit F S (1978) Geology and radioactive mineralization of Gebal El-Missikat area, Eastern Desert, Egypt, Ph. D. Thesis, Faculty of Science, Ein Shams University, Cairo, 289. P.
- Bakhit FS, Assaf HA, Dief AA (1985) Correlation study on the geology and radioactivity of surface and subsurface working at El Missikat area, Central Eastern Desert. *Egypt Mining Geol* 35(193):345–354
- Bakhit FS, Kassas IAE (1989) Distribution and orientation of radioactive veins in the El Erediya-El Missikat area, Central Eastern Desert Egypt. *Int J Remote Sensing* 10(3):565–581
- Ballouard C, Poujol M, Boulvais P, Mercadier J, Tartèse R, Venneman T, Deloule E, Jolivet M,
- Kéré I, Cathelineau M, Cuney M (2017) Magmatic and hydrothermal behavior of uranium in syntectonic leucogranites: The uranium mineralization associated with the Hercynian Guérande granite (Armorican Massif, France). *Ore Geol Rev* 80:309–331
- Bolonin AV, Gradovsky IF (2012) Supergene processes and uranium ore formation in the Ronneburg ore field Germany. *GeolOre Deposits* 54(2):122–131
- Bowden P, Herd D, Kinnaird JA (1995) The significance of Uranium and Thorium concentrations in pegamitic leucogranites (alaskites), Rössing Mine, Swakopmund. *Namibia Commun geol Surv Namibia* 10:43–49
- Boyle RW (1982) Deposits of Thorium and Uranium and their indicator elements. *Dev Econ Geol* 16:39–121
- Breiter K (2016) Monazite and zircon as major carriers of Th, U, and Y in peraluminous granites: examples from the Bohemian Massif. *Mineral Petrol* 110:767–785
- Burt DM (1989) Compositional and phase relations among rare earth element minerals geochemistry and mineralogy of rare earth elements mineral. *Soc Amer* 21:260
- Chiozzi P, Pasquale V, Verdoya M (2007) Radiometric survey for exploration of hydrothermal alteration in a volcanic area. *J Geochem Explor* 93:13–20
- Condomines M, Morand P, Allégre CJ (1981) ^{230}Th - ^{238}U radioactive disequilibria in tholeiites from the FAMOUS zones (Mid-Atlantic Ridge, $36^{\circ}50'\text{N}$): Th and Sr isotopic geochemistry. *Earth Planet Sci Lett* 55:247–256
- Condomines M, Morand P, Allégre CJ, Sigvaldason G (1981) ^{230}Th - ^{238}U disequilibria in historical lavas from Iceland. *Earth Planet Sci Lett* 55:393–406
- Cuney M (2014) Felsic magmatism and uranium deposits. *Bull Soc géol France* 185(2):75–92
- Darnley A G (1982) Hot Granites: Some General Remarks. In: Maurice, Y.T. (ed), Uranium in Granites. Proceedings of a workshop held in Ottawa, Ontario, Canada. Ministry of Supply and Services Canada, pp. 1–10.
- Deng T, Chi G, Zhang X, Li Z, Xu D, Li S, Du P, Shang P, Zou S, Zhou W, Xu K, Yan H, Wen M, Ding Z (2022) Mass Transfer during hematitization and implications for uranium mineralization in the zoujiashan deposit, xiangshan volcanic basin. *J Earth Sci* 33(2):422–434
- Dessouky OK, Ali HH (2018) Using portable gamma-ray spectrometry for testing uranium migration: a case study from the Wadi El Kareim Alkaline Volcanics, Central Eastern Desert Egypt. *Acta Geol Sinica* 92(6):2214–2232
- Dickson BL, Scott KM (1997) Interpretation of aerial gamma ray surveys-adding the geochemical factors. *J Aust Geol Geophys* 17(2):187–200
- Dongarra G (1984) Geochemical behaviour of uranium in the supergene environment. In: Vivo De et al (eds) Uranium geochemistry, mineralogy, geology, exploration and resources. The Institution of Mining and Metallurgy, Dordrecht
- El Tahir M A (1985) Radioactivity and mineralization of granitic rocks of El-Erediya occurrence and comparison to El Missikat-Rei El Garra occurrence, Eastern Desert, Egypt, Ph.D. Thesis, Faculty of Science, Al Azhar University, Cairo Egypt.132p.
- El-Kammar AM, El-Hazik N, Mahdi M, Aly N (1997) Geochemistry of accessory minerals associated with radioactive mineralisation in the central Eastern Desert Egypt. *J Afr Earth Sci* 25(2):237–252
- El-Kassas I A (1974) Radioactivity and geology of wadi Atalla area, Eastern Desert of Egypt, A.R.E. Ph. D. Thesis, Faculty of Science, Ein Shams University, Cairo, 502. P.
- Elkattan EM, Sadek HS, Rabie SI, Hassanein HI (1995) Ground geophysical study for development and exploration of El Missikat radioactive

- minerals prospect, central Eastern Desert of Egypt. *Nucl Geophys* 4(9):363–382
33. El-Leil IAA, Tolba AS, Omar SA, El-Feky MG, Bakiet MH, Awad HA (2015) Radioactive mineralization of El-Missikat granite; one of most important occurrence, eastern desert Egypt. *Int J Innov Sci Eng Technol* 2:83–100
 34. El-Sherif AM (2013) Mineralogical characterization of the alteration facies at Gabal El-Missikat Area, Central Eastern Desert. *Egypt Nuclear Sciences Scientific Journal* 2(1):1–21
 35. El-Tahir M A (1978) Relation between geology and radioactivity of some basement rock to the north of Qena-Safaga Asphaltic Road, Eastern Desert, Egypt, M. Sc. Thesis, Faculty of Science, Al Azhar University, Cairo, 148, P.
 36. Fall M, Baratoux D, Jessell M, Ndiaye PM, Vanderhaeghe O, Moyon JF, Baratoux L, Bonzi WM (2020) The redistribution of thorium, uranium, potassium by magmatic and hydrothermal processes versus surface processes in the Saraya Batholith (Eastern Senegal): Insights from airborne radiometrics data and topographic roughness. *J Geochem Explor* 219:1–18
 37. Förster HJ (1998) The chemical composition of REE-Y-Th-U-rich accessory minerals in peraluminous granites of the Erzgebirge Fichtelgebirge region, Germany, part I: the monazite-(Ce)-brabantite solid solution series. *Am Miner* 83:259–272
 38. Galbraith JH, Saunders DF (1983) Rock classification by characteristics of aerial gamma-ray measurements. *J Geochem Explor* 18:49–73
 39. Hassaan MM, Omar SA, Khalil AE, Shahin TM, El-Naggar IM, Sayyed MI, Hanfi MY (2022) Prognostic exploration of UF-Au-Mo-W younger granites for geochemical pathfinders, genetic affiliations, and tectonic setting in El-Ereidiya-El-Missikat Province, Eastern Desert. *Egypt Minerals* 12(5):518
 40. Honghai F, Jinyong C, Shengyun W, Jingyang Z, Dazhao G, Yanning M (2107) Genesis and Uranium Sources of Leucogranite-hosted Uranium Deposits in the Gaudeanmus Area, Central Damara Belt, Namibia: Study of Element and Nd Isotope Geochemistry. *ACTA GEOLOGICA SINICA* 91 (6), 2126–2137.
 41. Hussein H A M, Sayyah T A (1992) Uranium potential of the younger granites of Egypt (No. IAEA-TECDOC--650).
 42. Hussein H A, Hassan M A, El-Tahir M A, Abou-Deif A (1986) Uranium-bearing siliceous veins in younger granites, Eastern Desert, Egypt (No. IAEA-TECDOC--361).
 43. Ibrahim T M, Cuney M, El Agami N L, Meguid A A A, Zalata A K A (2004) Alteration processes and elements mobility in El Missikat granite, Eastern Desert, Egypt. In Proc. 6th Int. Conf. Geochem., Alexandria Univ., Egypt, VI-B (pp. 465–481).
 44. Killeen PG (1979) Gamma-Ray Spectrometric Methods in Uranium Exploration and Interpretation. *Geophysics and Geochemistry in the Search for Metallic Ores*, Edited by Hood PJ, Geological Survey of Canada Economic Geology Report 31, 163–230.
 45. Kirkland CL, Smithies RH, Taylor RJM, Evans N, McDonald B (2015) Zircon Th/U ratios in magmatic environs. *Lithos* 212:397–414
 46. Lentz DR (1991) Radioelement distribution in U, Th, Mo, and rare-earth-element pegmatites, skarns, and veins in a portion of the Grenville Province, Ontario and Quebec. *Can J Earth Sci* 28(1):1–12
 47. Leroy JL, Turpin L (1988) REE, Th and U behaviour during hydrothermal and supergene processes in a granitic environment. *Chem Geol* 68:239–251
 48. Maden N, Akaryali E (2015) Gamma ray spectrometry for recognition of hydrothermal alteration zones related to a low sulfidation epithermal gold mineralization (eastern pontides, NE türkiye). *J Appl Geophys* 122:74–85
 49. Mamouch Y, Attou A, Miftah A, Ouchchen M, Dadi B, Achkouch L, Ettayea Y, Allaoui A, Boualoul M, Randazzo G, Lanza S, Muzirafuti A (2022) Mapping of Hydrothermal Alteration Zones in the Kelâat M'Gouna Region Using Airborne Gamma-Ray Spectrometry and Remote Sensing Data: Mining Implications (Eastern Anti-Atlas, Morocco). *Appl Sci* 12(957):1–19
 50. Massey MS, Pacheco JSL, Nelson J, Fendorf S, Maher K (2014) Uranium Incorporation into Amorphous Silica. *Environ Sci Technol* 48(15):8636–8644
 51. Meisl S, Pöschl W (1982) Radioactive Disequilibrium studies in uranium occurrences of the Odenwald, West Germany. In: Amstutz GC, El Goresy A, Frenzel G, Kluth Moh, G, Wauschkuhn, A, Zimmemann, RA, (eds) Ore genesis special publication No 2 of the society for geology applied to mineral deposits. Springer-Verlag, Berlin, Heidelberg
 52. Mohammed AA (2001) Morphological and geochemical characteristics of zircon as a guide to uranium origin in El-Missikat and El-Ereidiya plutons, Central Eastern Desert Egypt. *J Facul Educ* 26(1):141–155
 53. Nagar MS, Kamal HM, El Monsif AM, Ghazala RA (2020) Potential uranium recovery by percolation leaching from El Missikat mineralized silica vein, Eastern Desert Egypt. *Academia J Environ Sci* 8(5):071–080
 54. Nash JT (1979) Uranium and thorium in granitic rocks of northeastern Washington and northern Idaho, with comments on uranium resource potential. U.S. Geol Survey Open-File Rep 79–233:1–47
 55. Nishimori R K, Ragland P C, Rogers J J W, Greenberg J K (1977) Uranium Deposits in Granitic Rocks. Energy Research and Development Administration Technical Report-GJBX-13 (77), Grand Junction, Colorado, pp.1–93.
 56. Osman AM, Salman AB, El-Mansi MM, Abdel Ghani IM, Abdallah SM (2005) Mineralogy and uranium distribution in some subsurface sections from El-Missikat and El-Ereidiya uranium occurrences, Eastern Desert. *Egypt Delta J Sci* 29:18–38
 57. Rabie SI, Abdel-Meguid AA, Assran AS (1998) Geological and geophysical exploration for uranium mineralization in the El-Ereidiya prospect Area, Central Eastern Desert. Egypt. Springer, Dordrecht
 58. René M (2020) Alteration of granitoids and uranium mineralization in the Blatná suite of the central bohemian plutonic complex. *Czech Republic Minerals* 10(821):1–18
 59. Rich RA, Holland HD, Petersen U (1977) Hydrothermal uranium deposits. Elsevier, Amsterdam
 60. Rogers JJW, Adams JAS (1978) Thorium and Uranium. In: Wedepohl KH, Correns CW, Shaw DM, Turekian KK, Zemann J (eds) *Handbook of Geochemistry* (II-5). Springer-Verlag, Berlin-Heidelberg-New York, pp 798–822
 61. Rubatto D (2017) Zircon: the metamorphic mineral. *Rev Mineral Geochem* 83:261–295
 62. Scharfenberg L, Regelous A, de Wall H (2019) Radiogenic heat production of Variscan granites from the Western Bohemian Massif, Germany. *J Geosci* 64:251–269
 63. Shalaby MH, Bishta AZ, Roz ME, El Zalaky MA (2010) Integration of geologic and remote sensing studies for the discovery of uranium mineralization in some granite plutons, Eastern Desert Egypt. *J King Abdulaziz Univ Earth Sci* 21(1):125
 64. Shives RBK, Charbonneau BW, Ford KL (2000) The detection of potassic alteration by gamma-ray spectrometry-recognition of alteration related to mineralization. *Geophysics* 65(6):2001–2011
 65. Shives R BK, Charbonneau BE, Ford KL (1997) The detection of potassic alteration by gamma-ray spectrometry—Recognition of alteration related to mineralization. In *Proceedings of Exploration 97: Fourth Decennial Conference on Mineral Exploration*, edited by A.G. Gubins, 741–752.
 66. Sobolev IS, Orekhov AN, Bratec T, Rikhvanov LP, Soboleva NP (2018) Variance—correlation analysis in the exploration of hydrothermal (fluidogenus) deposits using surface gamma-ray spectrometry. *J Appl Geophys* 159:597–604
 67. Uyanik NA, Öncü Z, Uyanik O, Bozcu M (2022) Determination of alteration zones and geological unit limits using natural radioactivity properties of sandikli-şuhut areas. *J Appl Geophys*. <https://doi.org/10.1016/j.jappge.2021.104525>
 68. Waber N, Schorscher HD, Tj P (1992) Hydrothermal and supergene uranium mineralization at the Osamu Utsumi mine, Poços de Caldas, Minas Gerais, Brazil. *J Geochem Explor* 45:53–112
 69. Wanggh G, Wang X, Chai X, Liu J, Deng N (2010) Adsorption of uranium (VI) from aqueous solution on calcined and acid-activated kaolin. *Appl Clay Sci* 47(3–4):448–451
 70. Yakymchuk C, Kirkland CI, Clark C (2018) Th/U ratios in metamorphic zircon. *J Metamorphic Geol* 36:715–737
 71. Zhai W, Zhang E, Zheng S, Santosh M, Sun X, Niu H, Fu B, Fu Y, Li D, Jiang Y, Liang F, Lin W, Zhao Y, Han S (2022) Hydrothermal zircon: characteristics, genesis and metallogenic implications. *Ore Geol Rev* 149:1–16

Publisher's Note

Springer Nature remains neutral with regard to jurisdictional claims in published maps and institutional affiliations.